ANALYSIS AND DESIGN OF A CIRCULARLY POLARIZED MICROSTRIP
ANTENNA

A THESIS SUBMITTED TO
THE GRADUATE SCHOOL OF NATURAL AND APPLIED SCIENCES
OF
MIDDLE EAST TECHNICAL UNIVERSITY

BY

MEHMET TAŞTAN

IN PARTIAL FULFILMENT OF THE REQUIREMENTS
FOR
THE DEGREE OF MASTER OF SCIENCE
IN
ELECTRICAL AND ELECTRONICS ENGINEERING

DECEMBER 2006

Approval of the Graduate School of Natural and Applied Sciences

_____
Prof. Dr. Canan ÖZGEN
Director

I certify that this thesis satisfies all the requirements as a thesis for the degree of Master of Science.

_____
Prof. Dr. İsmet ERKMEN
Head of Department

This is to certify that we have read this thesis and that in our opinion it is fully adequate, in scope and quality, as a thesis for the degree of Master of Science.

_____
Assoc. Prof. Dr. Sencer KOÇ
Supervisor

Examining Committee Members

Prof. Dr. Altunkan HIZAL (METU, EE) _____

Assoc. Prof. Dr. Sencer KOÇ (METU, EE) _____

Prof. Dr. Gülbin DURAL (METU, EE) _____

Assoc. Prof. Dr. Özlem ÇİVİ (METU, EE) _____

Dr. Özlem ŞEN (TÜBİTAK, Uzay Tek.Enst.) _____

I hereby declare that all information in this document has been obtained and presented in accordance with academic rules and ethical conduct. I also declare that, as required by these rules and conduct, I have fully cited and referenced all material and results that are not original to this work.

Name, Last name : Mehmet TAŞTAN

Signature   :

ABSTRACT

ANALYSIS AND DESIGN OF A CIRCULARLY POLARIZED MICROSTRIP
ANTENNA

TAŞTAN, Mehmet

M.S., Department of Electrical and Electronics Engineering

Supervisor: Assoc. Prof. Dr. Sencer KOÇ

December 2006, 99 pages

In this study we tried to design a microstrip antenna, to get a suitable radiation
pattern for a LEO satellite. Our aim is to get a radiation pattern that has a
maximum power which is not in the broadside direction to the antenna surface;
instead broadside radiation has a relatively lower power density. Maximum power
radiation is desired to be at about $30 - 50$ degrees angle beyond the normal to the
antenna surface. We desire circularly polarized radiation. We used two concentric
antennas; one is a circular patch at the center and the other is an annular ring
which is used at the outer region. By using Ansoft Ensemble 8.0 software, we
design an antenna which has a resonance frequency at 8.2 GHz. Using the result of
the program we design the real antenna. The measurement results are compared
with the simulation results.

Key words: circular patch, annular ring, edge port model, method of moment,
microstrip antennas, circularly polarized microstrip antenna.

ÖZ

DAİRESEL POLARİZASYONLU MİKROŞERİT ANTEN ANALİZ VE TASARIMI

TAŞTAN, Mehmet

Yüksek Lisans, Elektrik ve Elektronik Mühendisliği Bölümü

Tez Yöneticisi: Doç. Dr. Sencer KOÇ

Aralık 2006, 99 Sayfa

Bu çalışmada alçak yörünge uyduları için kullanılabilecek, uygun bir ışıma diyagramına sahip mikroşerit anten tasarımı yapılmıştır. Bu çalışmanın amacı; maksimum radyasyonu anten düzlemine dik istikamette değil de, anten düzlemi ile $30 - 50$ derece açı yapacak şekilde yayın yapan bir mikroşerit anten tasarlamaktır. Bu çalışmada dairesel polarizasyonlu bir radyasyon elde edilmiştir. İç içe geçmiş; biri disk, diğeri de bunu çevreleyen halka şeklinde iki anten kullanılmıştır. Ansoft Ensemble 8.0 yazılım programı kullanılarak 8.2 GHz. Frekansında, istenen radyasyona sahip bir anten simule edilmiştir. Bu programdan elde edilen verilere göre gerçek bir anten tasarlanmıştır. Sonuçta deneysel verilerle programdan elde edilen veriler mukayese edilmiştir.

Anahtar Kelimeler: Dairesel disk, halka anten, Kenar bağlantı noktası modeli, Momentler Yöntemi, Mikroşerit antenler, Dairesel polarizasyonlu mikroşerit antenler.

To My Wife

ACKNOWLEDGMENTS

TABLE OF CONTENTS

LIST OF FIGURES

LIST OF TABLES

CHAPTER 1

INTRODUCTION

Low Earth Orbit (LEO) satellites are being used widely for various applications in the world. Some of the main features of LEO satellites are that they are not geostationary which means that they are continuously in motion with respect to a stationary point on the Earth and that their velocity is related to the height of their orbit from the ground level. In communication area, there occur some problems if we try to use a classical beam shaped antenna on a LEO satellite because of the fact that a commonly used antenna, such as a microstrip patch operating in the dominant mode, has a radiation pattern with a maximum in the broadside direction. To overcome this problem a special type of antenna whose beam shape is given in Fig.1–1 is proposed. If the antenna beam shape is of this type the signal level will always be the same in a stationary earth station (e.g. for a Global Positioning System – GPS user). In other words, the motion of the satellite will not cause any problem since the earth station gets always the same level of signal from the satellite.

As for the geometry and statement of the problem mentioned above, considering the parameters shown in Fig.1–2 where the satellite boresight is shown to be aimed at the Earth, we can define:

$$\cos\theta = \frac{r^2 + h^2 + 2ah}{2r(a+h)} \qquad (1.1)$$

where h is the height of the satellite from the earth level and θ is the angle of the earth station with respect to the satellite antenna.
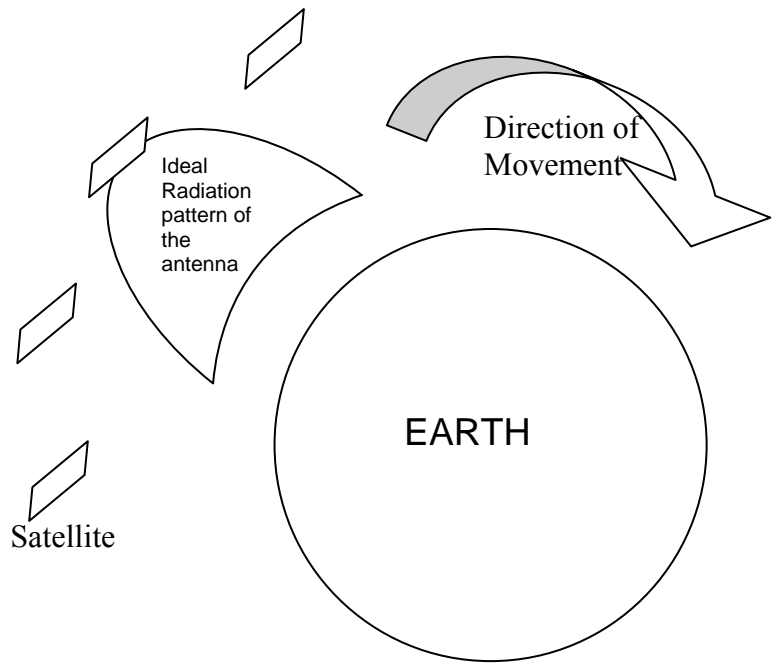
Figure 1–1 Ideal Radiation Pattern of an LEO Satellite Antenna.
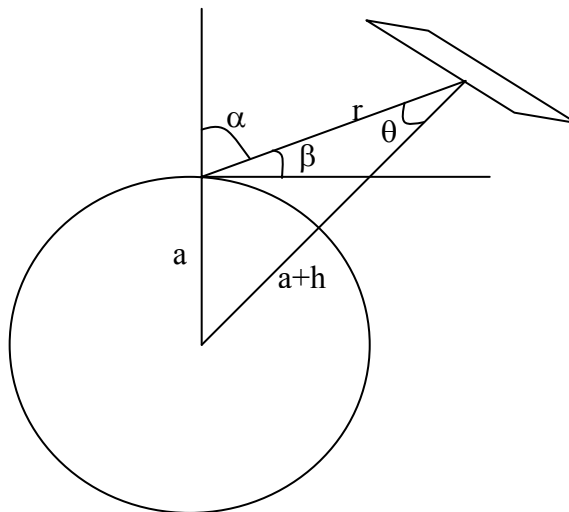
Figure 1–2 The Geometry of the problem

The power received by the user is

$$P_r = \frac{\lambda^2}{(4\pi r)^2} G_e G_s P_s \tag{1.2}$$

where

λ is the wavelength,

G_e is the earth station antenna gain,

G_s is the satellite antenna gain,

P_s is the satellite transmitter power.

The aim is to get a constant power when satellite moves or, in other words, r changes. Because earth station antenna is pointed towards the satellite at all times, the only changing parameters are the distance r and the angle θ. So it is required that:

$$\frac{G_s}{r^2} = C = const. \tag{1.3}$$

For a LEO satellite, it can be assumed that h<<a and in that condition, the satellite antenna has a secant^2 power pattern:

$$G_s(\theta) = G(0)\sec^2\theta \ \text{ for } 0<\theta<\theta_m \tag{1.4}$$

where θ is the elevation angle and θ_m is the angular limit up to which the beam is requested to follow a secant – squared shape. Beyond that angle, radiation pattern should drop to zero as fast as possible for a LEO satellite antenna.

An approximate power pattern is given in Fig.1–3 where G(0) is assumed to be 1.
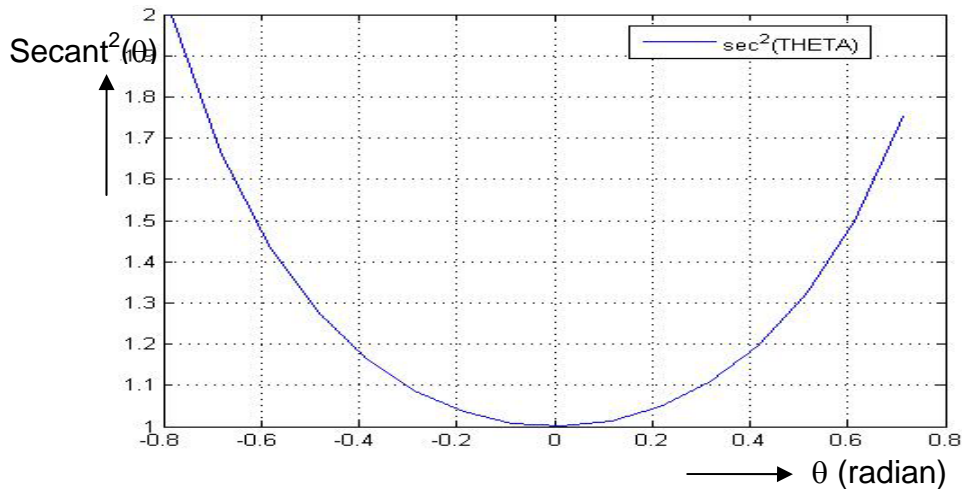
Figure 1–3 Secant-squared power pattern.

Since the location of the satellite is arbitrary with respect to the user station, it would be better to have a circularly polarized antenna. If satellite doesn't use circularly polarized radiation pattern, the user station must be rotated for polarization match.

In the literature, one can find numerous studies realized on the subject described above. Some of them are summarized below:

In [1] a circularly – polarized conical beam antenna has been designed to communicate between a mobile station and a stationary satellite. The radiation towards a desired direction was accomplished by using monopole antennas with simple structures at low cost.

Similar conical beam pattern obtained by using a microstrip structure was discussed in [2]. The peak of the conical pattern could be varied within a wide angular range by exciting the patch at different higher order modes and/or by loading the substrate with materials of different dielectric substrate.

4

Unipolar conical beam antennas using microstrip patch radiators in a ring formulation was studied in [3] for the same application. A dual polarized conical beam microstrip antenna was presented and realized as an array of three square patches whose corners meet at a central feed point.

The design and performance of two low gain shaped beam quadrifilar helix antennas – QHA's on a large complex spacecraft were presented in [4]. Cosinusoidal or conical shaped beams were designed using QHA's.

In this thesis, the same radiation pattern which was investigated in [4] is used. The main difference is that we tried to design the antenna by using a microstrip structure because of its low profile and suitability for space and mobile application.

The main reason of this study is to get a suitable radiation pattern for a LEO satellite antenna by using a microstrip structure. This thesis is composed of six main chapters and two appendices:

The first chapter is the introduction. The second chapter gives a detailed explanation of microstrip structure and its use. The third chapter explains the circular and annular microstrip structures in detail. The fourth chapter describes the circular disk annular ring microstrip – CDAR structure and the formulas needed to understand the design of our project. The fifth chapter presents the simulation and experimental results together with some discussions. The last chapter concludes this thesis.

CHAPTER 2

MICROSTRIP ANTENNAS

Microstrip antennas have been used extensively in the past 30 years, because of their light weight, suitability for space and mobile applications. Microstrip antennas are composed of mainly three sections: the ground plane, an insulating substrate material and the antenna section as given in Fig.2–1.

Radiating antenna section

Insulating dielectric material with relative permittivity ε_r

Conducting Ground Plane

h
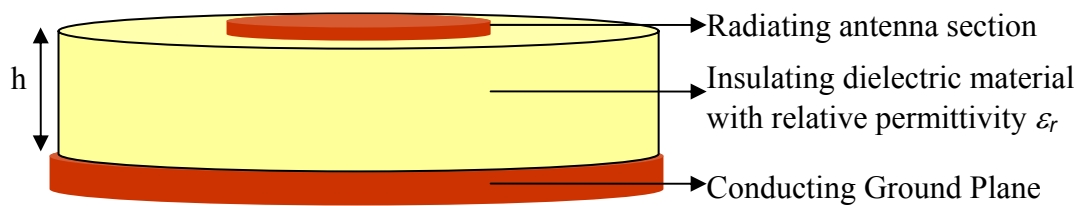
Figure 2–1 Typical microstrip antenna

2.1 Why we use microstrip antenna; advantages and disadvantages.

Microstrip antennas have been used in the frequency range from 100 MHz. to 100 GHz. Microstrip antennas, discussed in [5], have the following advantages:

a. Light weight, low volume and conformal to surfaces of some vehicles,

b. Low fabrication cost, so these antennas can be manufactured in large quantities,

c.	These antennas can be polarized both, linear as well as circular,

d.	Microstrip antennas can be easily integrated with microwave integrated circuits (MICs).

e.	Microstrip antennas are capable of dual and triple frequency operations.

f.	They can be manufactured mechanically robust when mounted on rigid surfaces.

Beyond these advantages, microstrip antennas have a number of disadvantages as compared to conventional antennas. The major disadvantages, discussed in [5], are given below:

a.	Narrow bandwidth (this can be increased by using thicker substrate),

b.	Lower transmitter power, up to about 100 W.

c.	Most of them radiate into the half space,

d.	Surface wave excitation decrease the efficiency,

e.	Cross polarization is high, and some other disadvantages are given in [5].

In our study we used a circular and annular microstrip antenna to get our idealized radiation pattern.

2.2 Radiation fields from a microstrip antenna

In microstrip transmission lines it is preferred to use a thin dielectric substrate with a high dielectric constant to decrease radiation. On the other hand, thick and lower dielectric constant substrates are preferred to increase efficiency of the microstrip antenna. Radiation from a rectangular patch can be explained with the fields that occur between the patch metallization and the ground plane.
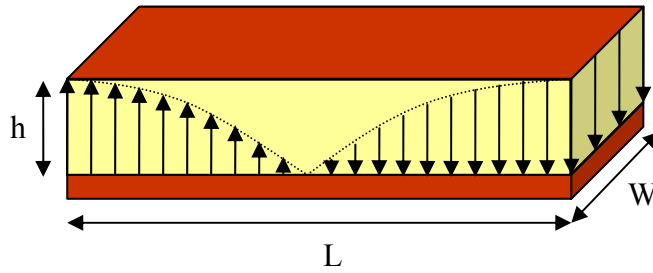
Figure 2–2 Electric field distributions in the microstrip cavity

Related formulas about the radiation field calculations are given in Appendix −A. Some feeding techniques of microstrip structure will be presented in the following subsection.

2.3 Feeding Techniques of Microstrip Antennas

Some feeding techniques are microstrip feed, coaxial feed, proximity coupled microstrip feed, aperture coupled microstrip feed and coplanar waveguide feed. For this study probe feed and microstrip feed techniques will be discussed in detail to explain our studies.

2.3.1 Coaxial Probe Feed

Coaxial probe feeding technique is shown in Fig.2–3 below.
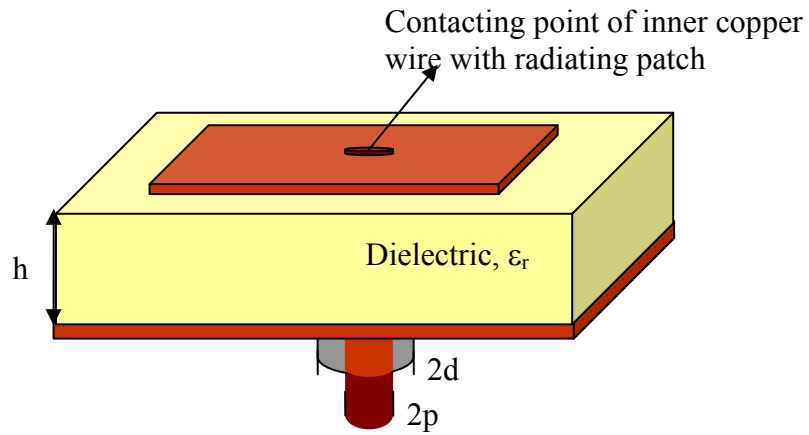
Figure 2–3 Coaxial feeding of microstrip antenna (p is the radius of the inner copper wire, d is the radius of the outer copper of the coaxial cable)

Probe position is adjusted to get the best matching condition. The coupling between the probe and the patch is obtained from the current J_z to the patch field E_z. Coupling for a rectangular patch is given by;

$$Coupling \cong \iiint_v E_z J_z dv \cong Cos(\pi x_0 / L) \tag{2.1}$$

where x_0 is the offset position from the patch edge, and L is the resonant length of the patch. [5]

Coaxial feeding technique is simple to adjust the position of probe. But if thicker substrate and many probe feeding is needed, this creates some problems. For example fabrication will be difficult and also reliability decreases in this condition. This increases spurious radiation from probe.

2.3.2. Microstrip Line Feeding

In this feeding technique, patch and feeding line both lie on the same surface; this results in the simple fabrication shown in Fig.2–4 below.
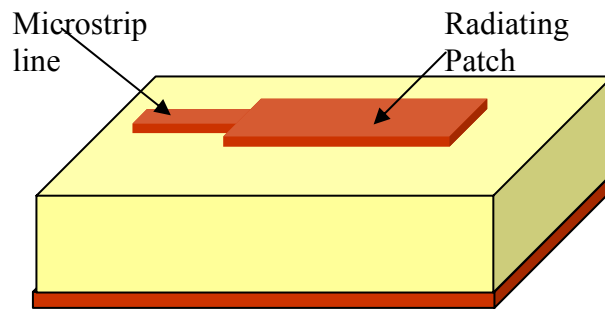
Figure 2–4 Microstrip line feeding of a patch

Modeling of equivalent circuit, Edge – coupled feeding design technique and Finite Difference Time Domain – FDTD technique based approaches of edge coupled feeding are given in [5].

Leaving the details of the formulations to the references, let's study a little more about circular and annular ring antennas in the next chapter.

CHAPTER 3

CIRCULAR DISK AND ANNULAR RING MICROSTRIP ANTENNAS

Circular antennas and ring antennas can be used in the same structure to get the antenna radiation pattern desired in this work. These two antennas must resonate in different modes. In this chapter circular and annular ring antennas are discussed in details.

3.1 Circular Disk Microstrip Antennas

Circular microstrip antennas can be analyzed using cavity model. A circular disk antenna is shown in Fig.3–1.
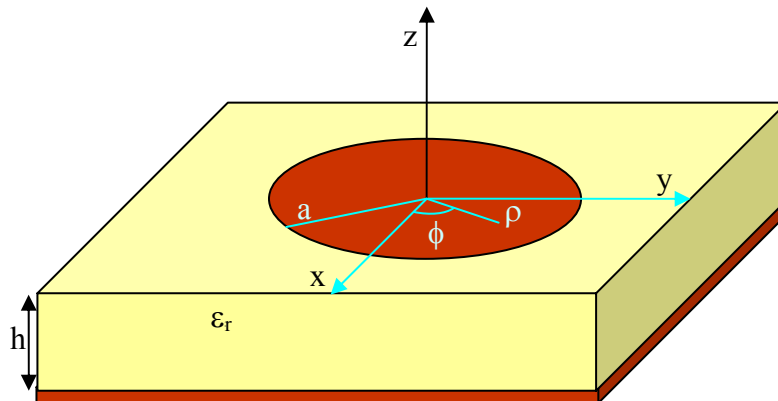
Figure 3–1 Circular disk microstrip antenna

The wave equation for the electric fields can be written as;

$$(\nabla^2 + k^2)\vec{E} = 0 \qquad k = 2\pi\sqrt{\varepsilon_r}/\lambda_0 \qquad (3.1)$$

In the cylindrical coordinate system, the wave equation has the solution,

$$E_z = E_0 J_n(k\rho)\cos n\phi \qquad (3.2)$$

where $J_n(k\rho)$ are the Bessel functions of order n. The details are given in Appendix – B.

Resonant frequency:

Resonant frequency of a circular disk antenna can be calculated for the TM_{nm} mode from the basic relation $\chi_{nm}=ka$. Using this relationship, the resonant frequency can be obtained by;

$$f_{nm} = \frac{\chi_{nm}c}{2\pi a_e\sqrt{\varepsilon_r}} \qquad (3.3)$$

where;

χ_{nm} is the mth zero of $J_n{'}(ka)$,

c is the velocity of light in free space,

a_e is the effective radius of the circular disk antenna. Some values of the roots of the χ_{nm} are given in the Table 3.1 below.

Table 3–1 The roots of $J_n{}'(ka)$

n \ m	0	1	2	3	4
1	0	1.84118	3.05424	4.20119	5.317
2	3.38171	5.331			

For TM_{11} mode of the circular disk antenna, the following formula has been suggested in [11] to determine the effective radius with an error of less than 2,5 % for $a/h \gg 1$;

$$a_e = a \left\{ 1 + \frac{2h}{\pi a \varepsilon_r} \left(\ln \frac{\pi a}{2h} + 1.7726 \right) \right\}^{1/2} \tag{3.4}$$

For an edge fed antenna, measured input resistance is always maximum. On the other hand, we must use a feeding point that match the impedance of the feeding line (this generally equals to 50Ω, unless otherwise determined) to get a minimum reflection.

If we use a probe feeding, the circular disk antenna is divided into two regions according to the probe position. [11]

In the first region (i.e. $\rho < \rho_0$);

$$E_z = \sum_{n=0}^{\infty} A_n J_n(k\rho) \cos n\phi, \tag{3.5a}$$

$$H_\rho = \frac{1}{jw\mu_0\rho} \sum_{n=0}^{\infty} nA_n J_n(k\rho) \sin n\phi, \tag{3.5b}$$

$$H_\phi = \frac{k}{jw\mu_0\rho} \sum_{n=0}^{\infty} A_n J'_n(k\rho) \cos n\phi \,, \tag{3.5c}$$

In the second region (i.e. $\rho > \rho_0$);

$$E_z = \sum_{n=0}^{\infty} [B_n J_n(k\rho) + C_n Y_n(k\rho)] \cos n\phi \tag{3.6a}$$

$$H_\rho = \frac{1}{jw\mu_0\rho} \sum_{n=0}^{\infty} n[B_n J_n(k\rho) + C_n Y_n(k\rho)] \sin n\phi \,, \tag{3.6b}$$

$$H_\phi = \frac{k}{jw\mu_0} \sum_{n=0}^{\infty} [B_n J'_n(k\rho) + C_n Y'_n(k\rho)] \cos n\phi \,, \tag{3.6c}$$

In Eqs.3-5 through 3-6 constant coefficients A_n, B_n and C_n are determined by using mode matching technique at $\rho = \rho_0$

E_z and H_ρ are continuous at $\rho = \rho_0$, which yields:

$$A_n J_n(k\rho_0) = B_n J_n(k\rho_0) + C_n J_n(k\rho_0) \tag{3.7}$$

H_ϕ is discontinuous at the same point, that is;

$$\frac{k}{jw\mu_0} \sum_{n=0}^{\infty} [B_n J'_n(k\rho_0) + C_n Y'_n(k\rho_0) - A_n J'_n(k\rho_0)] \cos n\phi = I_s \tag{3.8}$$

I_s is the z-directed feed current at $\rho = \rho_0$. For a thin probe with constant current I_p and located at (ρ_0, ϕ), then the I_s is;

$$I_s = I_p \delta(\phi) / \rho_0$$

Then we can write the unknown parameters for A_n, B_n and C_n as follows;

14

$$A_n = \frac{-jw\mu_0 I_p}{2(1+\varepsilon_n)} \frac{1}{D_n} \{J_n(k\rho_0)[Y_n'(ka) + j\eta_1 y_{sn} Y_n(ka)] - D_n Y_n(k\rho_0)\} \qquad (3.9a)$$

$$B_n = \frac{-jw\mu_0 I_p}{2(1+\varepsilon_n)} \frac{1}{D_n} J_n(k\rho_0)[Y_n'(ka) + j\eta_1 y_{sn} Y_n(ka)] \qquad (3.9b)$$

$$C_n = \frac{jw\mu_0 I_p}{2(1+\varepsilon_n)} J_n(k\rho_0) \qquad (3.9c)$$

where;

$$D_n = J_n'(ka) + j\eta_1 y_{sn} J_n(ka) \qquad (3.9d)$$

$$\eta_1 = \frac{120\pi}{\sqrt{\varepsilon_r}}$$

For a circular disk antenna of radius a, radiated field components of the dominant mode TM_{11} are given below;

$$E_\theta = -jV\frac{ak_0}{2}\frac{e^{-jk_0 r}}{r}\cos\theta J_1'(k_0 a \sin\theta) \qquad (3.10a)$$

$$E_\phi = jV\frac{ak_0}{2}\frac{e^{-jk_0 r}}{r}\frac{J_1(k_0 a \sin\theta)}{k_0 a \sin\theta}\cos\theta\sin\phi \qquad (3.10b)$$

The radiation pattern of the TM_{11} mode has a maximum and that of TM_{21} mode has a null in the broadside direction. The radiated fields are linearly polarized for only one probe feeding.

Neither of these modes has desired characteristics; however these structures are quite simple to fabricate and operate. Either mode can be used as the satellite antenna if simplicity is preferred over performance.

Let's simply explain other parameters; like radiated power, polarization and so on.

Radiated Power;

Radiated power can be calculated using the formula given below;

$$P_r = \frac{1}{2\eta_0} \int\limits_0^{2\pi} \int\limits_0^{\pi/2} (|E_\theta|^2 + |E_\phi|^2) r^2 \sin\theta d\theta d\phi \qquad (3.11)$$

By using numerical technique given in [2] we can get;

$$P_r = \frac{(E_0 h)^2 \pi^3 a^2}{2\lambda_0^2 \eta_0} \left[\frac{4}{3} - \frac{8}{15}(k_0 a)^2 + \frac{11}{105}(k_0 a)^4 - ... \right]$$

Polarization of a Circular Disk Microstrip Antenna

Normally for a one point probe feeding of a circular disk microstrip antenna, we get linear polarization. However, circularly polarized radiation is also possible by using one probe feeding but a little different shaped antenna must be used in that case.

Another method for circular polarization is to use two or four probe feeding with equal amplitude but 90° phase difference between each probe.

The advantage of using four probe feed is to suppress unwanted modes. To preserve beam symmetry and keep cross polarization low, especially for relatively thick substrate radiators, the unwanted modes need to be suppressed. As a general case the two neighboring modes of a resonant mode have the highest magnitudes. One way to suppress these adjacent modes is to employ four – feed probes located at geometrically symmetrical positions. These four feeds should have a phase arrangement of 0°, 90°, 0°, 90° for the even order modes and 0°, 90°, 180°, 270°

for the odd order modes so that the fields of the unwanted modes from the two opposing feeds cancel. The detailed explanations about these ideas are given in [2]. Assuming that only TM_{11} mode is excited from these four – feeds, electrical fields can be written as;

$$E_\theta^s(\theta,\phi) = E_\theta(\theta,\phi) + jE_\theta(\theta,\phi+\pi/2) - E_\theta(\theta,\phi+\pi) - jE_\theta(\theta,\phi+3\pi/2) \quad (3.12a)$$

$$E_\phi^s(\theta,\phi) = E_\phi(\theta,\phi) + jE_\phi(\theta,\phi+\pi/2) - E_\phi(\theta,\phi+\pi) - jE_\phi(\theta,\phi+3\pi/2) \quad (3.12b)$$

Where

$$E_\theta(\theta,\phi) = [J_2(k_0a\sin\theta) - J_0(k_0a\sin\theta)]\cos\phi \qquad (3.13a)$$

$$E_\phi(\theta,\phi) = [J_2(k_0a\sin\theta) + J_0(k_0a\sin\theta)]\cos\theta\sin\phi \qquad (3.13b)$$

and $k_0 = 2\pi f/c$ is the free space wave number. The equations are then

$$E_\theta^s(\theta,\phi) = 2[J_2(k_0a\sin\theta) - J_0(k_0a\sin\theta)](\cos\phi - j\sin\phi) \qquad (3.14a)$$

$$E_\phi^s(\theta,\phi) = 2j[J_2(k_0a\sin\theta) + J_0(k_0a\sin\theta)]\cos\theta(\cos\phi - j\sin\phi) \quad (3.14b)$$

and if θ dependent terms are approximately equal for θ and ϕ components of the fields, the pattern will be circularly polarized. In that case we have

$$k_0a = \frac{k_{11}a}{\sqrt{\varepsilon_r}} = \frac{\chi_{11}}{\sqrt{\varepsilon_r}} = \frac{1.84118}{\sqrt{\varepsilon_r}} \qquad (3.15)$$

and if the substrate is known the patterns can be easily calculated. The patterns simulated by Ansoft Ensemble 8.0 software are shown in Fig.3–4.

In our project we also design the circular and annular section for circularly polarized radiation. Phase differences must be adjusted for each probe appropriately. The probe feeding magnitude and phases are shown in the Fig.3–3 below;
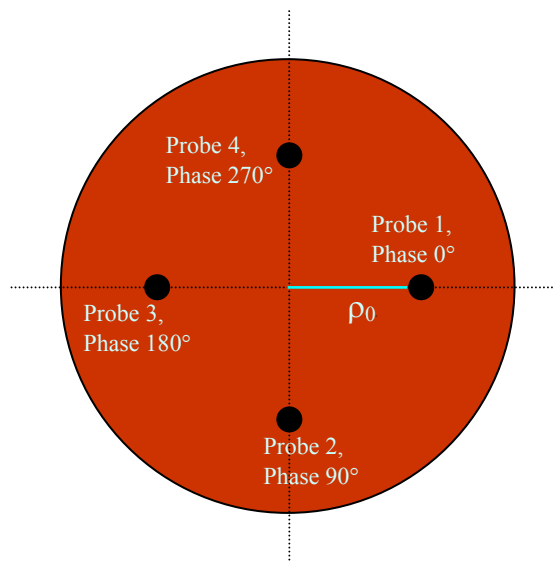
Figure 3–2 Four probe feed phase relation for TM_{11} mode to get circular polarization

Investigating Fig.3–3, we see that the maximum radiation is in the broadside direction and also cross polarization is low (about 20 dB in the related region)
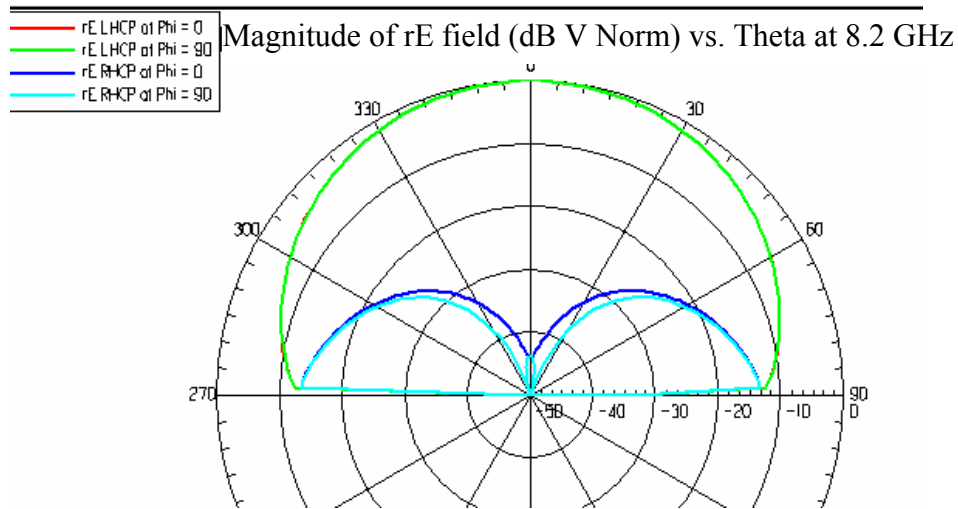
Figure 3–3 Magnitude of rE field (dB, Normalized) vs. θ at 8.2 GHz. (Ansoft Ensemble 8.0)

3.2. Annular Ring Microstrip Antennas

Annular ring antennas have some useful features; resonant modes can be adjusted by controlling the ratio of the outer radius to the inner radius. It is possible to operate in two different frequencies by using two concentric antennas; one is circular disk at the inner side and the other is an annular ring at the outer section of the antenna.

In this thesis we also used two concentric antennas operating at the same resonant frequency, but at different modes.

An Annular ring microstrip antenna is shown in Fig.3–4 below. It comprises a ring – shaped conductor on one side of a dielectric substrate with a ground plane on the other side. The structure resonates at discrete frequencies given in [8]

19
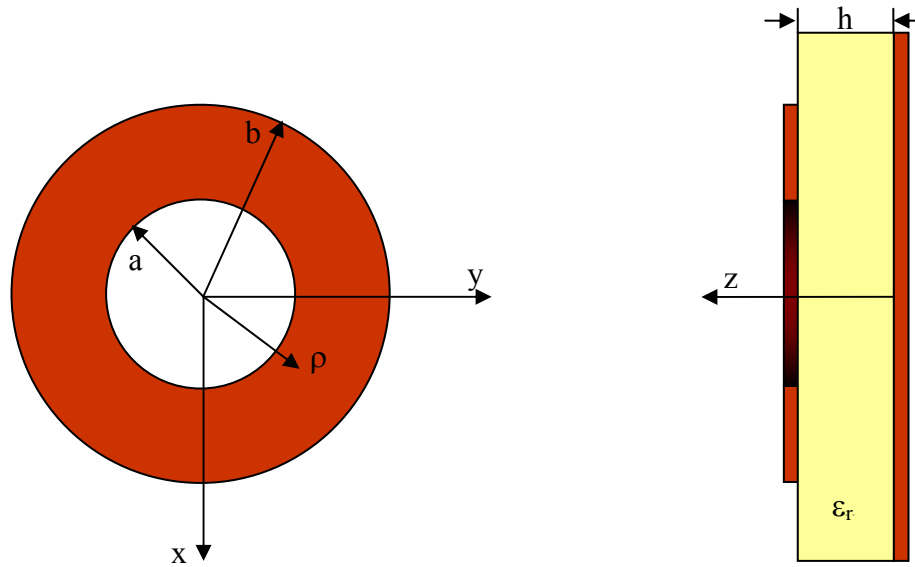
Figure 3–4 Geometry of an annular ring microstrip antenna

Radiation field components are calculated using the formula below; [11]

$$E_z = E_0[J_n(k\rho)Y_n'(ka) - J_n'(ka)Y_n(k\rho)]\cos n\phi \tag{3.16a}$$

$$H_\rho = \frac{j}{w\mu\rho}\frac{\partial E_z}{\partial \phi}, \tag{3.16b}$$

$$H_\phi = -\frac{j}{w\mu}\frac{\partial E_z}{\partial \rho} \tag{3.16c}$$

Inside the cavity; the other field components are zero.

The surface current on the lower surface of the ring is;

$$\vec{J}_s = -\hat{z} \times \vec{H} = -\hat{\phi} H_\rho + \hat{\rho} H_\phi \tag{3.17}$$

and writing it in the other form we get;

$$J_\phi = \frac{j\eta E_0}{w\mu\rho} [J_n(k\rho)Y_n'(ka) - J_n'(ka)Y_n(k\rho)] \sin n\phi \tag{3.18a}$$

$$J_\rho = \frac{-jkE_0}{w\mu} [J_n'(k\rho)Y_n'(ka) - J_n'(ka)Y_n'(k\rho)] \cos n\phi \tag{3.18b}$$

At $\rho = a$ and $\rho = b$ radial component of the surface current must vanish to satisfy the magnetic wall boundary conditions so that;

$$J_\rho(\rho{=}b){=}H_\phi(\rho{=}b) \tag{3.19}$$

$$J_n'(kb)Y_n'(ka) - J_n'(ka)Y_n'(kb) = 0 \tag{3.20}$$

If *a, b, ε_r* and *n* are known, the roots of the above formula can be found.

For an approximate calculation; $k_{n1}a = 2an/(a+b)$ for $n \leq 5$

$(b-a)/(b+a) < 0{,}35$

Resonant frequency;

The resonant frequency is obtained by setting;

$k = \chi_{nm}/a$

or $f_{nm} = \dfrac{\chi_{nm}c}{2\pi a\sqrt{\varepsilon_r}}$ \hspace{2cm} (3.21)

21

In the above formula no fringing field is taken into account. In order to include the effect of fringing field effective dielectric constant ε_{re} can be used instead of ε_r. So we get an approximate expression for the resonance frequency as;

$$f_{nm} = \frac{\chi_{nm} c}{2\pi a \sqrt{\varepsilon_{re}}}$$
(3.22)

Fringing fields can be taken into account by considering an antenna that is wider than the physical width of the antenna. This is shown in the Fig.3–5 where w is the physical width of the antenna and w_e is the effective width of the antenna.
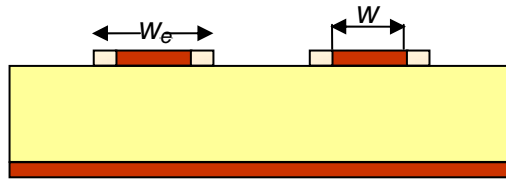
Figure 3–5 Fringing field consideration

Modified values of inner and outer radii of the annular ring antenna are given as;

$$a_e = a - (w_e - w)/2$$
(3.23a)

$$b_e = b + (w_e - w)/2$$
(3.23b)

Empirical formulas for a_e and b_e for the inner and outer effective radii of the annular ring antenna are given as; [8]

22

$$a_e = a - 3h/4 \tag{3.24a}$$

$$b_e = b + 3h/4 \tag{3.24b}$$

where h is the thickness of the substrate material. If thickness is very small then we can use as $a_e \approx a$ and $b_e \approx b$.

As a computation guideline; given a and b, first of all one can calculate a_e and b_e using the formula (3.24a, 3.24b), then find the χ_{nm} using the formula (3.20), and then calculate the resonant frequency of the annular ring antenna.

Radiation Fields:

Radiation fields of an annular ring microstrip antenna can be calculated from;

- The surface electric current distribution of the annular ring or,

- The magnetic current formulation,

We can use equivalent magnetic current formulation due to its simplicity.

Radiation fields are calculated independently at $\rho = a$ and $\rho = b$ from the magnetic currents and these two fields added vectorially to get the radiation fields of the microstrip ring antenna. [11]

$$E_\theta = j^n k_0 h \frac{e^{-jk_0 r}}{r} \left[a E_{zn}(a) J_n'(k_0 a \sin\theta) - b E_{zn}(b) J_n'(k_0 b \sin\theta) \right] \cos n\phi \tag{3.25a}$$

$$E_\phi = -n j^n k_0 h \frac{e^{-jk_0 r}}{r} \left[a E_{zn}(a) \frac{J_n(k_0 a \sin\theta)}{k_0 a \sin\theta} - b E_{zn}(b) \frac{J_n(k_0 b \sin\theta)}{k_0 b \sin\theta} \right] \cos\theta \sin n\phi$$

$$\tag{3.25b}$$

where;

$$E_{zn}(a) = E_0\left[J_n(k_{nm}a)Y_n'(k_{nm}a) - J_n'(k_{nm}a)Y_n(k_{nm}a)\right] = \frac{2E_0}{\pi k_{nm}a} \qquad (3.25c)$$

$$E_{zn}(b) = E_0\left[J_n(k_{nm}b)Y_n'(k_{nm}a) - J_n'(k_{nm}a)Y_n(k_{nm}b)\right] = \frac{a}{b}\frac{2E_0}{\pi k_{nm}a}\frac{J_n'(k_{nm}a)}{J_n'(k_{nm}b)} \qquad (3.25d)$$

$$E_\theta = j^n\frac{2E_0}{\pi k_{nm}}k_0 h\frac{e^{-jk_0 r}}{r}\left[J_n'(k_0 a\sin\theta) - \frac{J_n'(k_{nm}a)}{J_n'(k_{nm}b)}J_n'(k_0 b\sin\theta)\right]\cos n\phi \qquad (3.26a)$$

$$E_\phi = -nj^n\frac{2E_0}{\pi k_{nm}}k_0 h\frac{e^{-jk_0 r}}{r}\left[\frac{J_n(k_0 a\sin\theta)}{k_0 a\sin\theta} - \frac{J_n'(k_{nm}a)}{J_n'(k_{nm}b)}\frac{J_n(k_0 b\sin\theta)}{k_0 b\sin\theta}\right]\cos\theta\sin n\phi$$

$$(3.26b)$$

where $k_{nm}a = \chi_{nm}$

For the ratio of $b/a = 2$ some values of χ_{nm} are given in Table 3.2 below. χ_{12} is shown in bold character because this value will be used for our annular antenna section design.

Table 3–2 The roots of the function $J_n'(2\chi_{nm})Y_n'(\chi_{nm}) - J_n'(\chi_{nm})Y_n'(2\chi_{nm}) = 0$

m	1	2	3	4	5
n					
0		3.1966	5.6123	9.4445	12.5812
1	0.6773	**3.2825**	5.6532	9.4713	12.6012
2	1.3406	3.5313	6.4747	9.5516	12.6612

For the ratio of $b/a = 2.5$ some values of χ_{nm} are given in Table 3.3 below.

Table 3–3 Roots of the function $J'_n(2.5\chi_{nm})Y'_n(\chi_{nm}) - J'_n(\chi_{nm})Y'_n(2.5\chi_{nm}) = 0$

m	1	2	3	4	5
n					
0		…	…	…	…
1	0.5847	**2.2635**	4.273	6.339	….
2	1.1369	2.5665	4.4225	6.4365	….

For the ratio of $b/a = 3$ some values of χ_{nm} are given in Table 3.4 below.

Table 3–4 The roots of the function $J'_n(3\chi_{nm})Y'_n(\chi_{nm}) - J'_n(\chi_{nm})Y'_n(3\chi_{nm}) = 0$

m	1	2	3	4	5
n					
0		…	…	…	…
1	0.5136	**1.7578**	3.3261	….	….
2	0.9775	2.0901	3.4065	…	….

For m odd, TM_{1m} modes inner and outer fringing fields are of opposite polarity, giving rise to less radiation because of destructive interference,

For m even, TM_{1m} modes inner and outer fringing fields are of same polarity, giving rise to good radiation modes.

If the ratio of b/a increases, the directivity of the antenna will increase.

Annular ring antennas for circular polarization have been studied in [6] through [10]. Most of them used only one feeding point with an ear on the annular ring. In our thesis we used 4 feeding points in annular section for circular polarization to suppress the other modes defined in [2].

The pattern of a single annular ring antenna cannot be made to have local minima in the broadside direction by adjusting its parameters. However, a combination of a circular ring and a circular disk can be used to obtain the desired pattern.

In this chapter we derive the formulas for circular disk antennas and annular ring antennas as separate antennas. In the next chapter we derive the formulas for a concentric antenna; circular disk annular ring antenna which is composed of a circular disk at the center and an annular ring at the outer section.

CHAPTER 4

CIRCULAR DISK ANNULAR RING MICROSTRIP ANTENNA

In chapter 3 we analyzed circular disk microstrip antenna and annular ring microstrip antenna separately. In this chapter we analyze the circular disk annular ring – CDAR microstrip antenna with united construction on a single ground plane; in other words; circular disk is the inner part and annular ring is the outer part of the antenna. CDAR antenna structure is shown in the Fig.4–1 and 4–2.
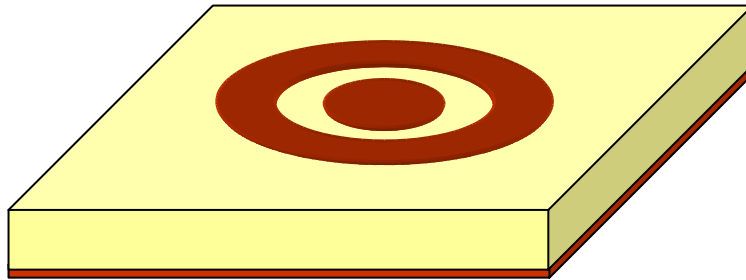

Figure 4–1 CDAR Antenna 3–dimensional view.

CDAR antennas can be used for different purposes; for example to get dual frequency operations. In this condition inner part operates at one frequency, outer part operates at another frequency.
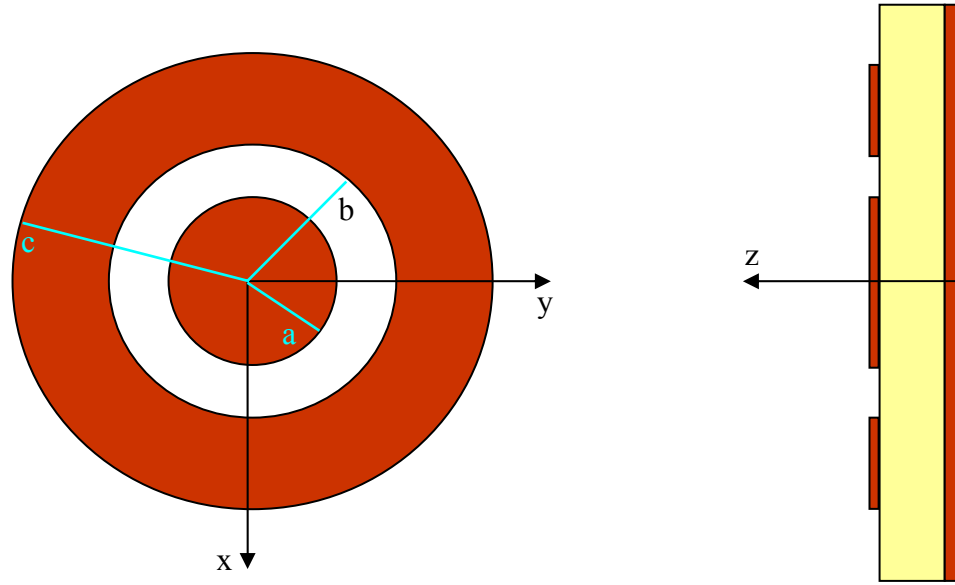
Figure 4–2 CDAR Antenna 2–dimensional view.

In our project we also used CDAR antenna to obtain the desired radiation pattern for Low Earth Orbit – LEO satellite antenna. But to get such a radiation pattern inner and outer parts of the CDAR antenna must operate at different modes. If inner part operates in TM_{11} mode with amplitude A, outer part operates in TM_{12} mode with amplitude B; the total radiation fields can be written as;

$$E_\theta(\theta,\phi) = \cos\phi \left[AJ_1'(k_0 a\sin\theta) - B\left(J_2'(k_0 b\sin\theta) - \frac{J_2'(k_{nm}b)}{J_2'(k_{nm}c)} J_2'(k_0 c\sin\theta) \right) \right]$$

(4.1a)

$$E_\phi(\theta,\phi) = \sin\phi\cos\theta \left[A\frac{J_1(k_0 a\sin\theta)}{k_0 a\sin\theta} - B\left(\frac{J_2(k_0 b\sin\theta)}{k_0 b\sin\theta} - \frac{J_2'(k_{nm}b)}{J_2'(k_{nm}c)} \frac{J_2(k_0 c\sin\theta)}{k_0 c\sin\theta} \right) \right]$$

(4.1b)

28

In this study, we want to get a radiation pattern; which has a maximum field strength that is not perpendicular to the antenna surface. By changing A and B; we can obtain a maximum field strength with an inclination angle $\alpha°$ from the antenna surface which is the coverage area of the satellite antenna. This ideal radiation pattern is shown in the Fig.1–2 in the first chapter.

To get the radiation pattern for idealized antenna; inner circular disk must be in TM_{11} mode and outer annular ring section must be in TM_{12} mode, but each section must resonate at the same frequency which is chosen as 8.2 GHz. In this study to simplify mathematical calculation we can use superposition principle, in other words, first of all calculate the radiation fields that comes from inner circular section, then calculate the radiation fields that comes from annular section of the antenna and then add these two fields to find the total fields. But to use this principle we must choose optimum values of parameters *a, b* and *c*. Investigating Tables 3.2 through 3.4 we can chose a *c/b* ratio of 2.5 to get an ideal and simple calculation. It is seen from Table 3.4 that *c/b* can not be chosen as 3. Because in that condition annular ring section will be smaller than that of circular radius, this can not be physically constructed. On the other hand, if we choose a *c/b* ratio of 2, annular ring section will be larger which is not desirable. So in this study we have chosen a *c/b* ratio between 2 and 3.

In the next chapter we discuss the solutions we got by using Ansoft Ensemble 8.0 software and then experimental results and comparison of experimental and simulation results.

CHAPTER 5

RESULTS AND DISCUSSIONS

In this chapter, the CDAR antenna with the desired characteristics has been designed. First, the antenna geometry is calculated using the results from chapter 3. Then the resulting design has been analyzed with the simulation program Ansoft Ensemble 8.0 software. Subsequently, the antenna geometry is refined using the simulation results, until the desired radiation pattern is reached. Finally, the resulting antenna design is implemented and the simulation results are compared with the experimental measurements.

5.1 Simulation with Ansoft Ensemble 8.0

Equations (4.1a) and (4.1b) give the electric field of a CDAR antenna.

Our aim is to design an antenna which has a resonance at 8.2 GHz. To get the ideal antenna pattern we choose $c/b = 2.5$ and a duroid substrate with a dielectric constant $\varepsilon_r = 2.2$ and a thickness of 0.127 mm. The relatively low thickness of the substrate leads to a negligible fringing field effect, so $a_e \approx a$, $b_e \approx b$ and $c_e \approx c$. Circular ring section is in TM_{11} mode and the annular ring section is in TM_{12} mode. Using (3.3) and (3.22) the antenna geometry can be calculated as;

$$a = \frac{1.84118 \times 3 \times 10^8}{2\pi \times 8.2 \times 10^9 \sqrt{2.2}} = 7.23 \text{ mm}$$

$$b = \frac{2.2635 \times 3 \times 10^8}{2\pi \times 8.2 \times 10^9 \sqrt{2.2}} = 8.9 \text{ mm}$$

$$c = 2.5 \text{ x } 8.9 = 22.25 \text{ mm}.$$

30

Initially the antenna is fed with 8 different probes. The Circular section is fed with an amplitude of one at each probe but with a 90° phase difference between each probe, similarly, the annular ring section is fed with an amplitude of 0.2 at each probe and the same phase difference between each probe. The antenna geometry, the frequency response and the radiation pattern are shown in Figs.5–1 through 5–5.

The simulation results displayed in Fig.5–4 indicate that the port 1 displayed in Fig.5–1 has a resonance frequency of 7.8 GHz, instead of the desired resonance frequency of 8.2 GHz. Similarly it is seen that the port 5 resonates at 8.05 GHz. Furthermore, the simulation results show that there is a coupling between the 1st and 3rd probes and also between the 5th and 7th probes. Thus the antenna geometry has to be refined to reach the desired antenna characteristics.
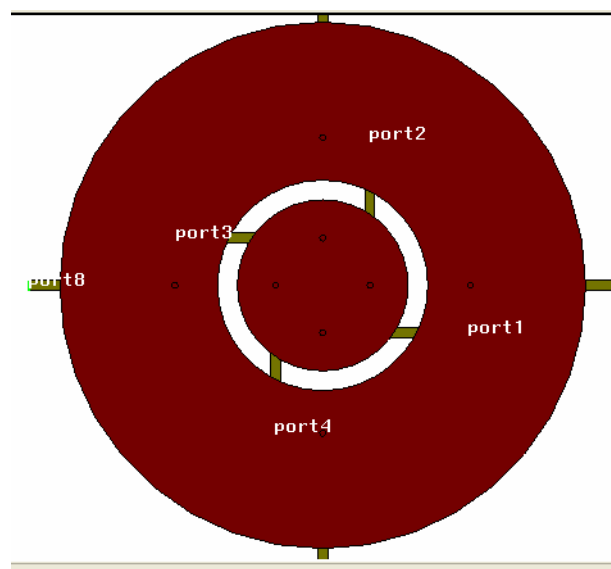

Figure 5–1 CDAR antenna top view; *a=7.23, b=8.9, c=22.25* mm.
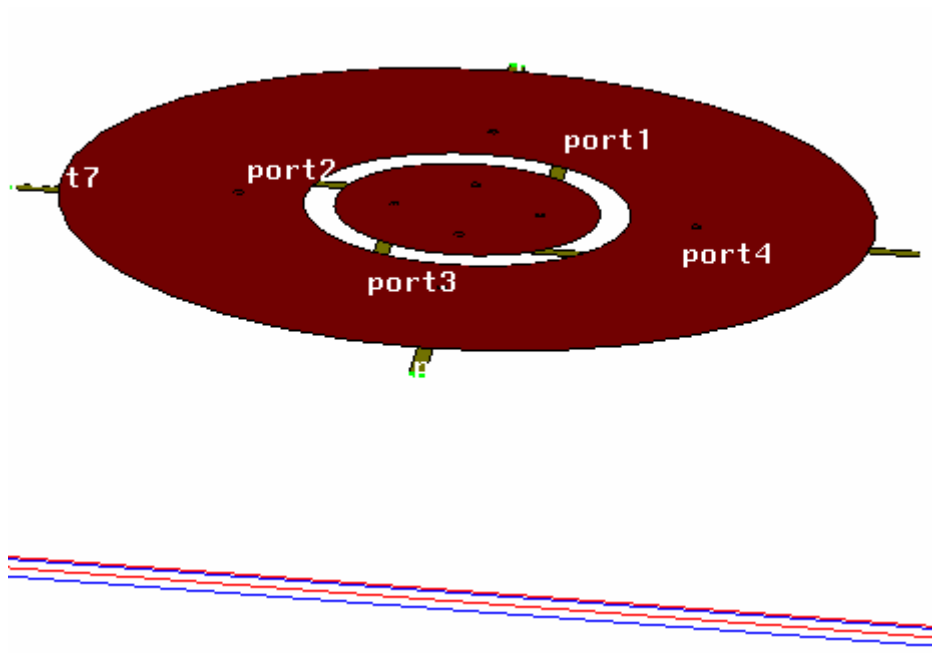
Figure5–2 CDAR antenna 3–dimensional view; *a=7.23, b=8.9, c=22.25* mm.
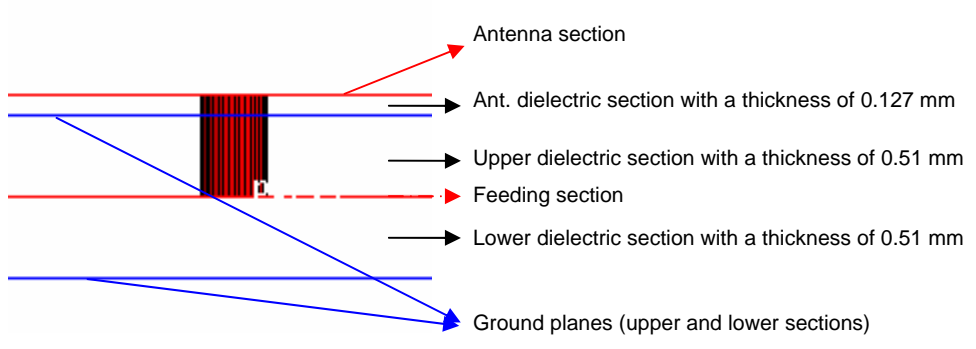
Figure 5–3 CDAR antenna side view
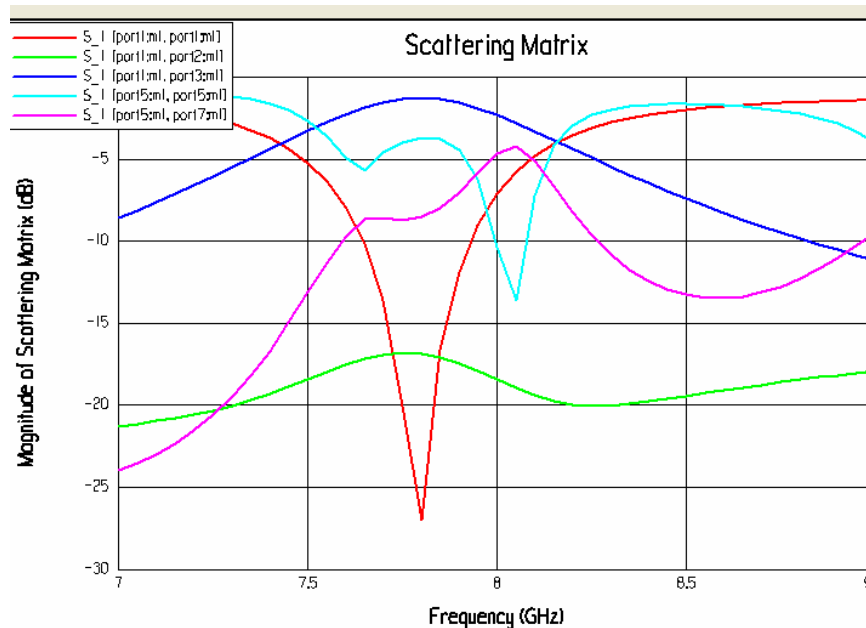
Figure 5–4 CDAR antenna scattering parameters versus frequency graph.

Simulation of the antenna structure shown in Fig.5-1 and 5-2 using Ansoft Ensemble 8.0 results in the far field radiation pattern displayed in Figs.5-5 to 5-7. (The circular section is fed with amplitude 1 at each probe and the annular section is fed with 0.2 at each probe at 7.8 GHz.) The simulation results show a discrepancy compared to the desired and the theoretically calculated antenna characteristics. The radiation pattern and the resonant frequency differ considerably. However, at 8.05 GHz, the simulation result approaches the desired radiation pattern.
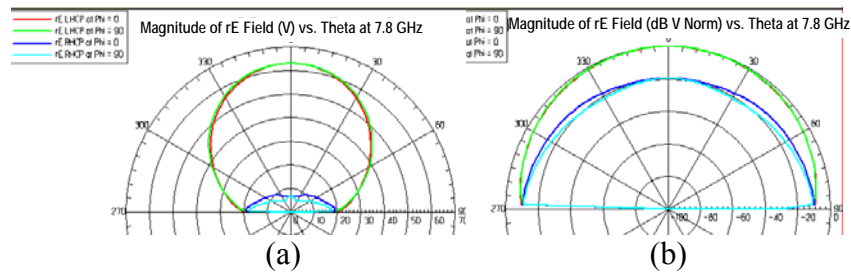
Figure 5–5 Radiation pattern at 7.8 GHz. (Exactly nice circular polarization, but not the idealized pattern. Also antenna efficiency, as explained in Appendix B, is good enough, 98,5 %)

Fig.5-5(a) displays the normalized pattern and 5-5(b) displays the pattern in dB. The antenna pattern at 8.05 GHz is also displayed in Fig.5-6, which shows a pattern very similar to the desired one, however, the antenna efficiency decreases to 74% from 98.5%. Thus the antenna geometry has to be modified to reach the desired antenna characteristics.

The new values for *a, b* and *c* can be calculated by proportional calculation; if 7.23 mm gives us 7.8 GHz, what must be the value of *a* to get 8.2 GHz. resonance. By a simple calculation one gets, a = 6.9, b = 8.7 and c = 21.8 mm. Using these values in the Ansoft Ensemble 8.0 simulation software results in the antenna characteristics displayed in Figs.5-7 and 5-8.
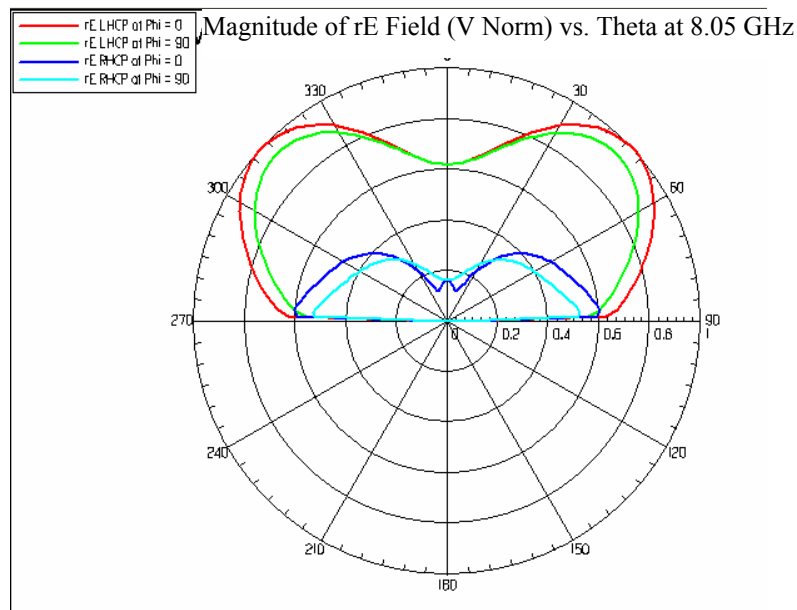
Figure 5–6 Radiation pattern at 8.05 GHz. (Efficiency is 74 %)

It is understood from Fig.5–8 that S_{11} does not have a minimum at 8.2 GHz as desired. To overcome this problem the circular section dimension must be modified a little more to achieve the ideal resonance condition. After some calculations we choose the value of *a* to be 6.84 mm. In that condition the circular and the annular sections come to resonance at 8.2 GHz. For these values of *a, b* and *c* (*a = 6.84, b = 8.7 and c = 21.8* mm.) we get the scattering versus frequency as displayed in Figs.5–9 and 5.10 and also the radiation pattern in Fig.5–11.
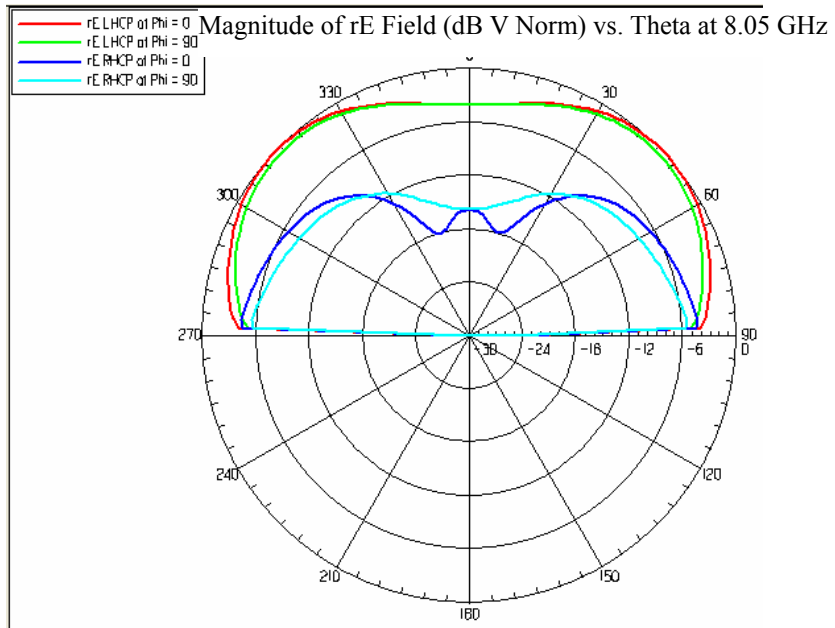
Figure 5–7 Radiation pattern at 8.05 GHz. (dB scale)
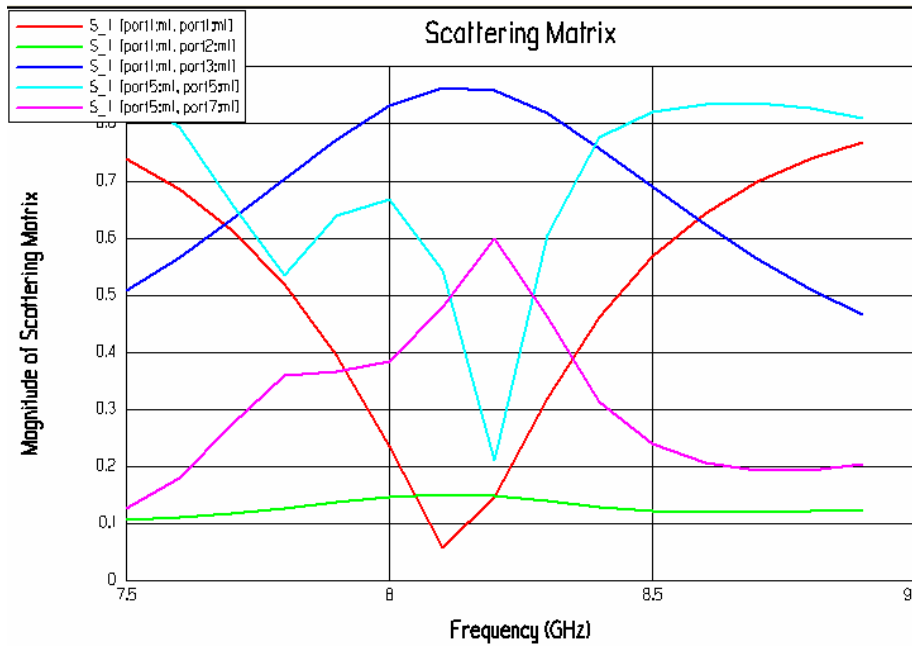
Figure 5–8 Frequency versus scattering parameter graph. (Linear scale)
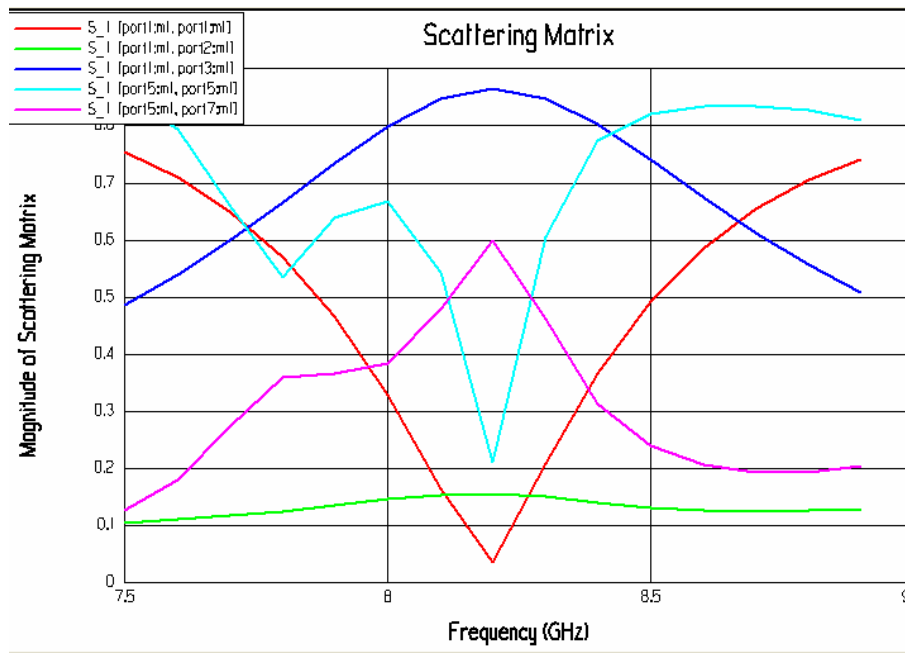
Figure 5–9 Frequency versus scattering parameter graph. (Linear scale - *a = 6.84 mm., b = 8.7 mm* and *c = 21.8 mm*)
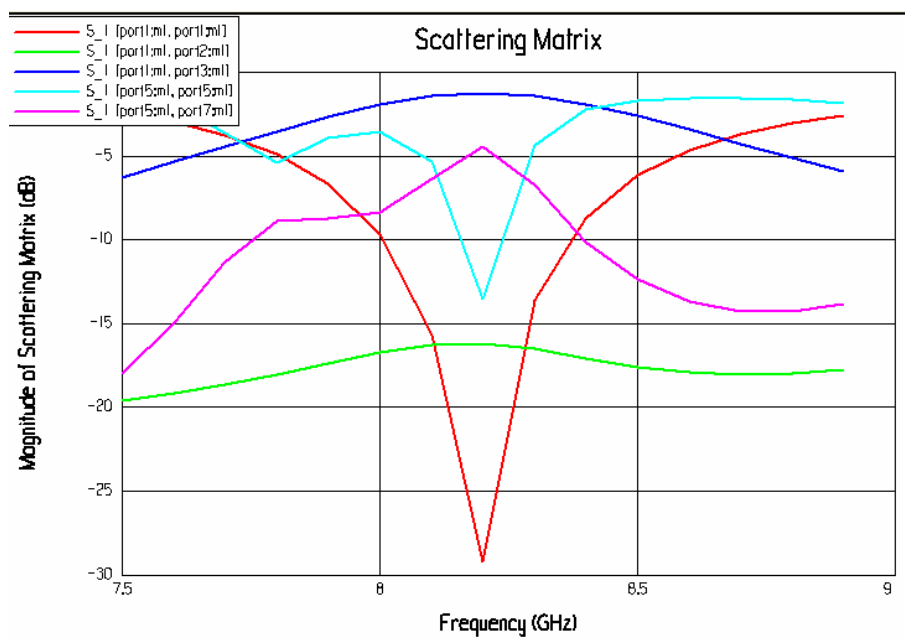

Figure 5–10 Frequency versus scattering parameter graph. (Logarithmic scale)
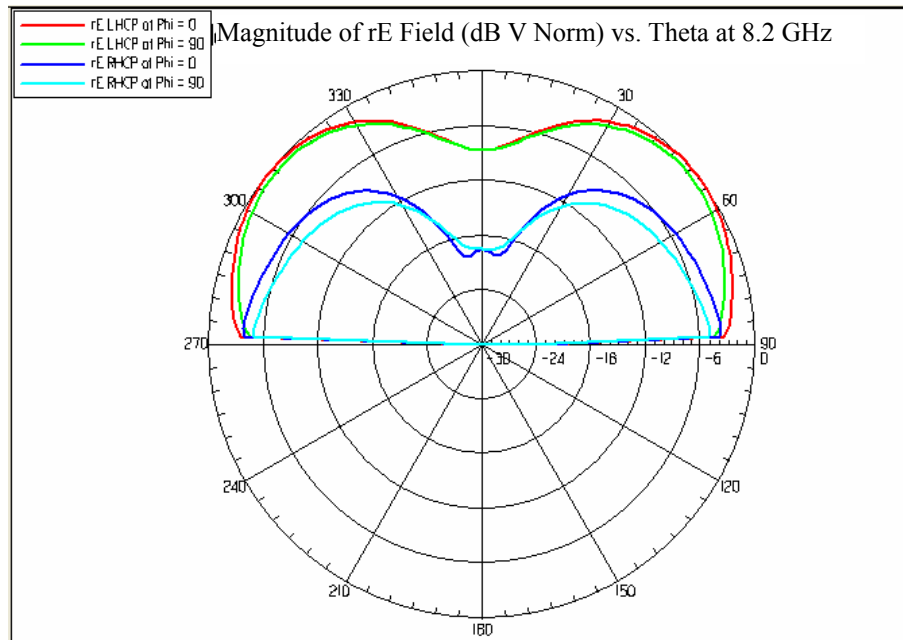
Figure 5–11 Far – Field Radiation pattern in dB scale (*a=6.84, b=8.7, c=21.8* mm. and circular sections are fed at ρ_{01}= *4* mm. and annular sections are fed at ρ_{02}=*12.5* mm.

It is seen from Fig.5–9 that both the circular and the annular sections resonate at 8.2 GHz. If we excite the circular sections with an amplitude of 1, and the annular sections with amplitude 0.2, we get a Far – Field radiation pattern as shown in Fig.5–11. This is the idealized radiation pattern for the LEO satellite antenna. The cross polarization is also low enough in the target region. Efficiency of the antenna is 99% at 8.2 GHz.

In the previous simulations, we fed all 8 ports separately. Our aim is to feed all 8 ports from one point. First we try to combine two ports to one port, leading to a total of 4 ports instead of 8 ports. To get a circular polarization, the line length must be adjusted to get 90° phase difference. Furthermore, the total port impedance is required to be 50 Ω. To this end, we use two parallel lines with 100 Ω impedance each, resulting in 50 Ω when combined. λ/4 length sections are used

for impedance transformation; that transforms the impedance from 50 Ω to 100Ω. We used two separate feeding sections; one for circular section and the other for annular section. Feeding sections are shown in Fig.5–13 and 5 – 14 separately. All substrates are duroid, (ε_r=2.2) with a thickness of 0.127mm for the antenna section, and 0.51mm for the feeding section.

duroid substrate thickness 0.51 mm
duroid substrate thickness 0.51 mm
duroid substrate thickness 0.51 mm
duroid substrate thickness 0.51 mm
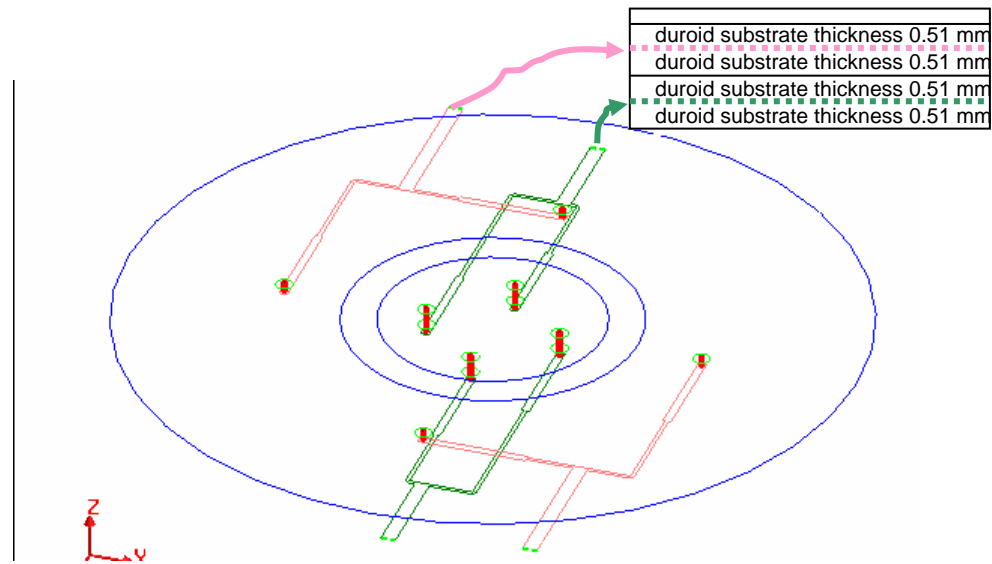
Figure 5–12 3–dimensional view of the antenna

Antenna frequency versus scattering parameter graph is shown in Fig.5–15.
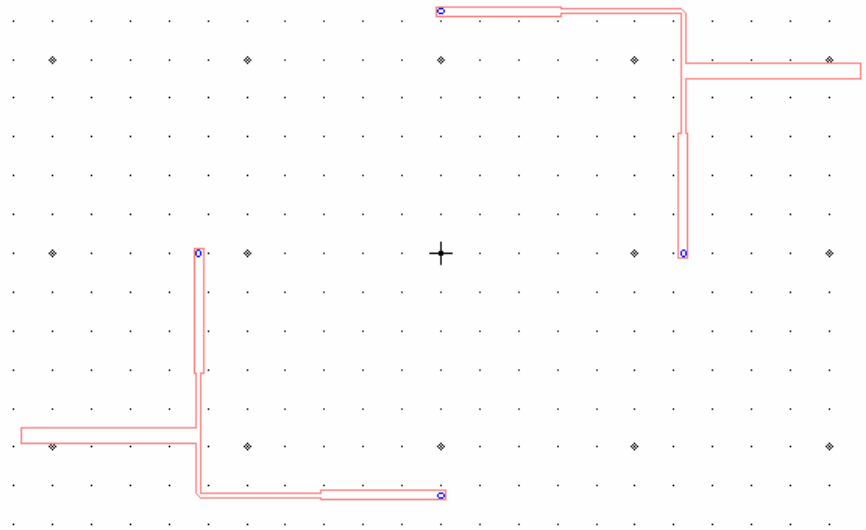
Figure 5 – 13 Annular ring feeding section
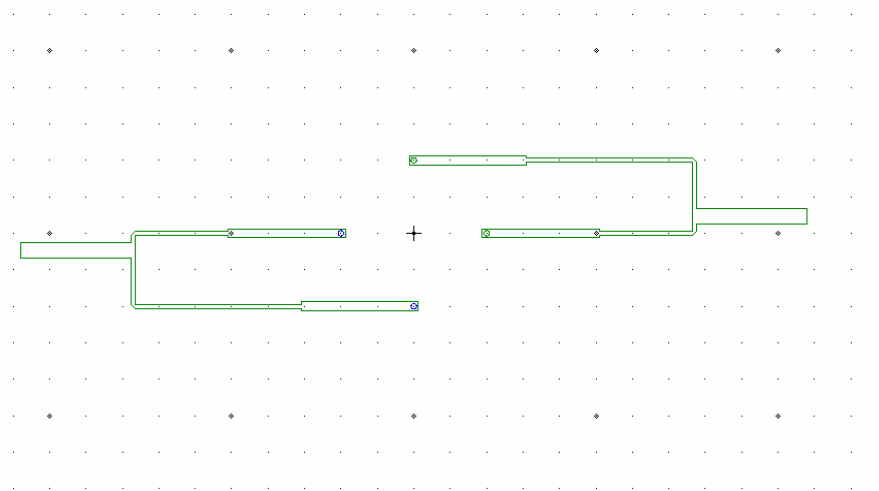
Figure 5–14 Circular disk feeding section
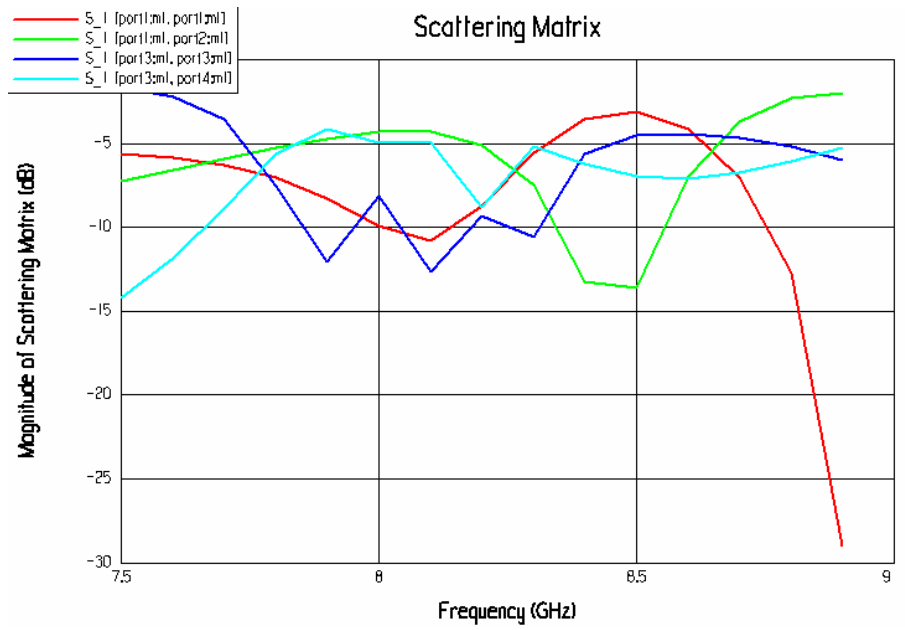
Figure 5–15 Frequency versus scattering parameter graph.
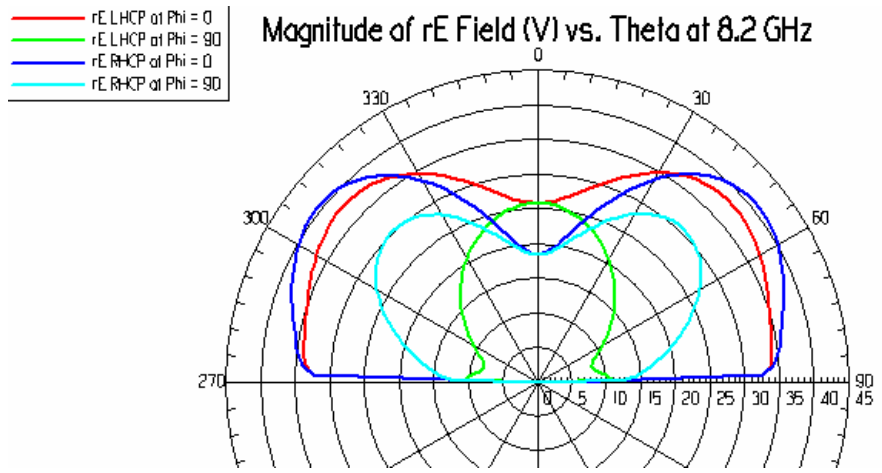
Figure 5–16 Far–field radiation pattern of the antenna

It is seen From the Fig.5–16 that the radiation pattern is very similar to the design specification, but the cross polarization is much higher than expected. This may be the result of the interaction between the edge port feeding of the ports 1 and 2 from the same edge. Another interesting result is the efficiency of the antenna which is 78 % at 8.2 GHz. We see a decrease in the efficiency because of the merging of the two ports.

Subsequently; we combine the upper and lower ports in one port, resulting in a total of two feeding ports, instead of 4. Upper and lower sections are not of equal impedances; they are chosen to be different selected to get the desired radiation pattern. The circular section is transformed from 50 Ω to 60 Ω, the annular section is transformed from 50 Ω to 300 Ω. Parallel connections of these two impedances is equal to 50 Ω. The other parameters for that antenna are as follows; dimensions of the antenna; a=6.84 mm., b=8.7 mm. and c=21.8 mm. feeding radius'; for circular section ρ_{01}=4 mm. and annular section ρ_{02}=12.5 mm to get the best matching condition.

The 3 – Dimensional view of the antenna, the scattering parameter graph and the radiation pattern of the antenna are shown in Figs.5–17 to 5–21.
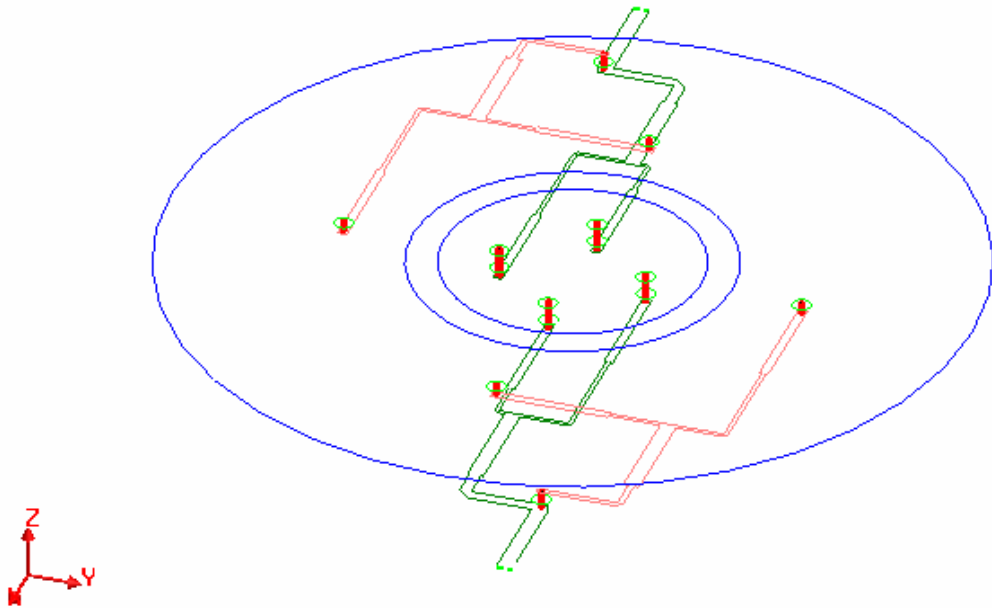
Figure 5–17 The 3–dimensional view of the antenna (feeding from 2 ports)

Figure 5–18 Frequency versus scattering parameter (dB scale)

f=8.1 GHz.
P_{in}=98 W.
P_{rad}=85 W.
e_r=87%
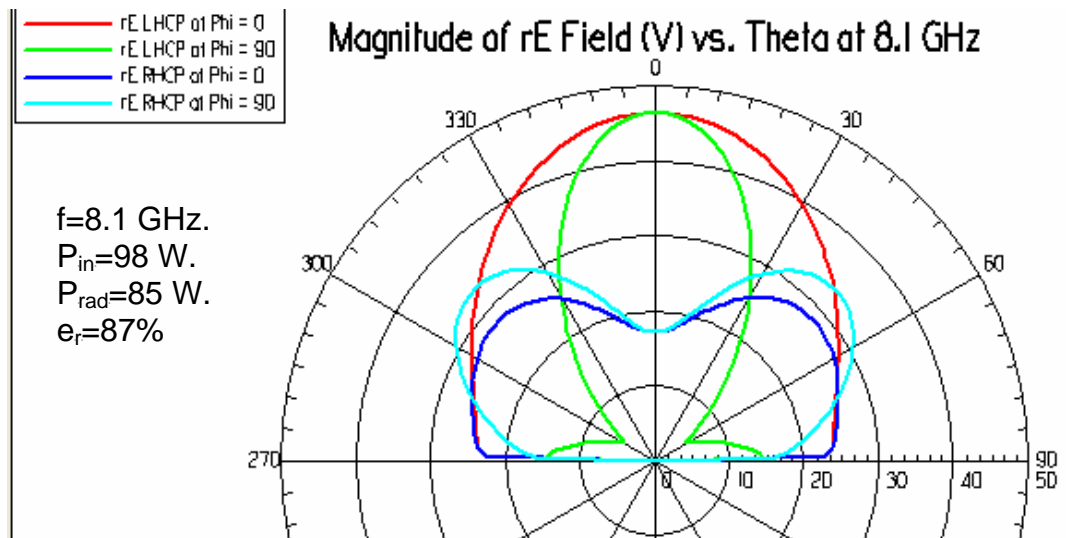
Figure 5–19 Far–field radiation pattern at 8.1 GHz.

f=8.2 GHz.
P_{in}=98 W.
P_{rad}=78 W.
e_r=80%
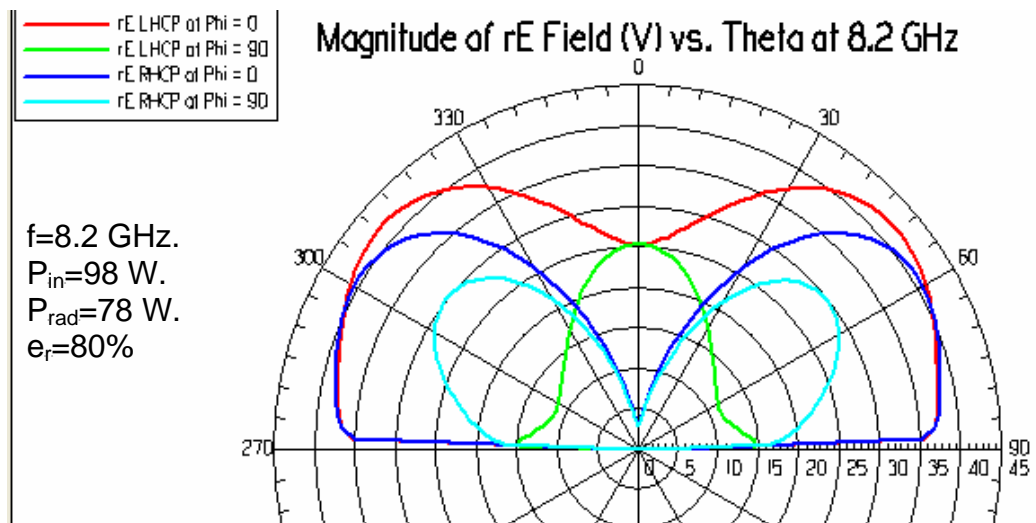
Figure 5–20 Far–field radiation pattern at 8.2 GHz.
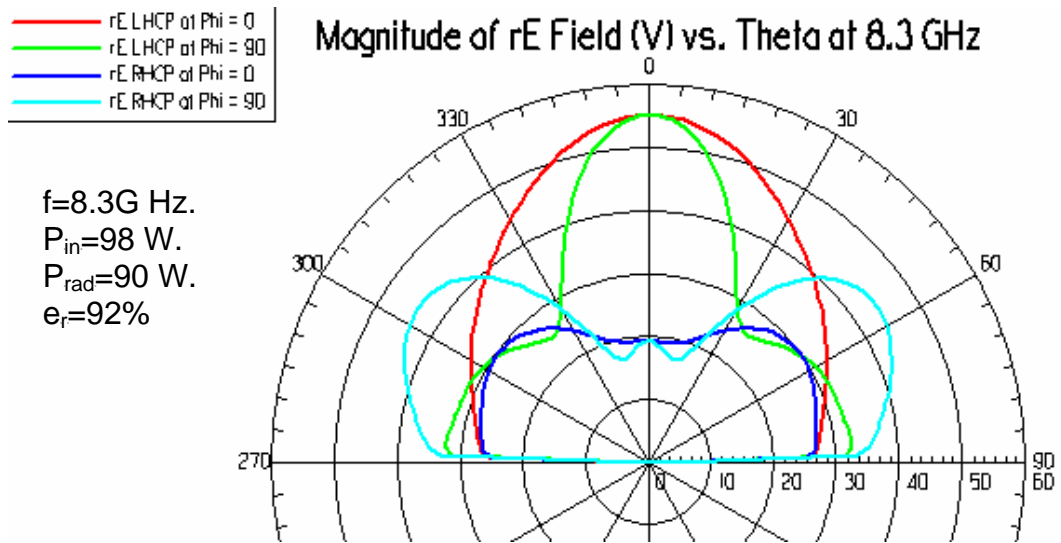
Figure 5–21 Far–field radiation pattern at 8.3 GHz.

By analyzing Figs.5–18 to 5-21 we see that the radiation patterns are similar to the desired pattern, however, the cross polarization is much larger than expected. Also, we understand that merging of ports results in decreased antenna efficiency.

To reach the desired 1–port antenna, we use the same antenna geometry as in the previous case, and merge the two remaining ports as shown in Fig.5–22. (i.e. a = 6.84 mm., b = 8.7 mm. and c = 21.8 mm. Circular feeding sections are all $\rho_{01} = 4$ mm. and annular sections $\rho_{02} = 12.5$ mm.). Circular ports are converted from 50 Ω to 60 Ω and annular sections are converted from 50 Ω to 300 Ω and the resulting impedance is 50 Ω. The 3 – dimensional view of the antenna, the feeding sections, the scattering pattern and the radiation pattern are shown in Figs.5–22 to 5–28.
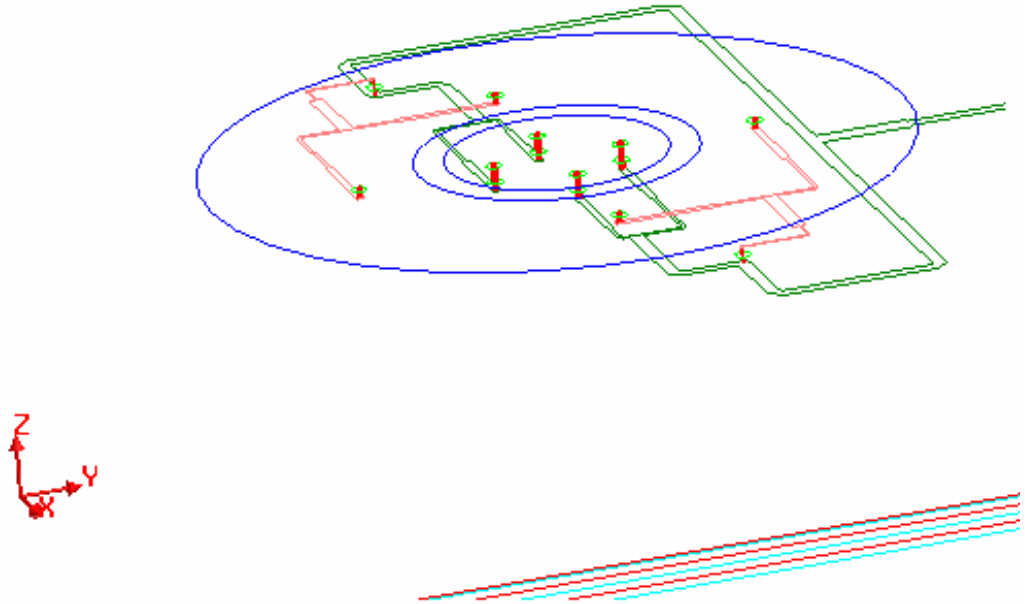
Figure 5–22 The 3–dimensional view of the antenna (All ports were merged to feed the antenna from only on point.). The Upper feed section feeds annular antenna, the downward feed section feeds the circular antenna. Impedance transformers are used to get the total port impedance to 50 Ω.

Figure 5–23 Circular antenna feeding section.

Figure 5–24 Annular ring antenna feeding section.
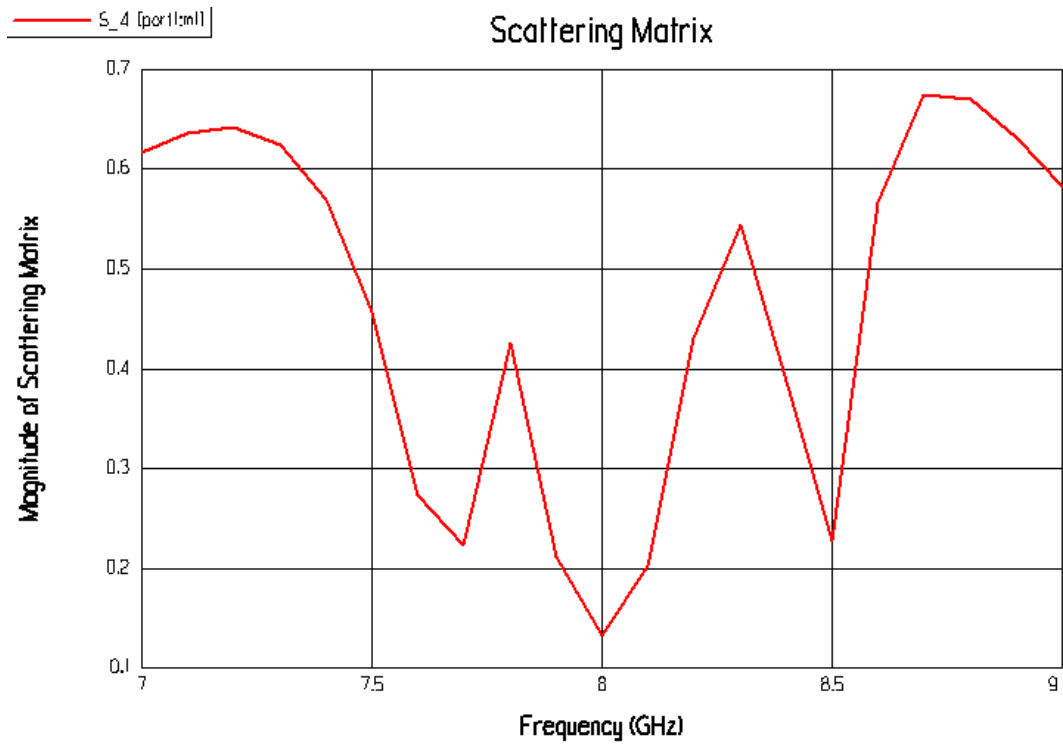
Figure 5–25 Scattering parameter versus frequency graph of the project that has only one feed point.
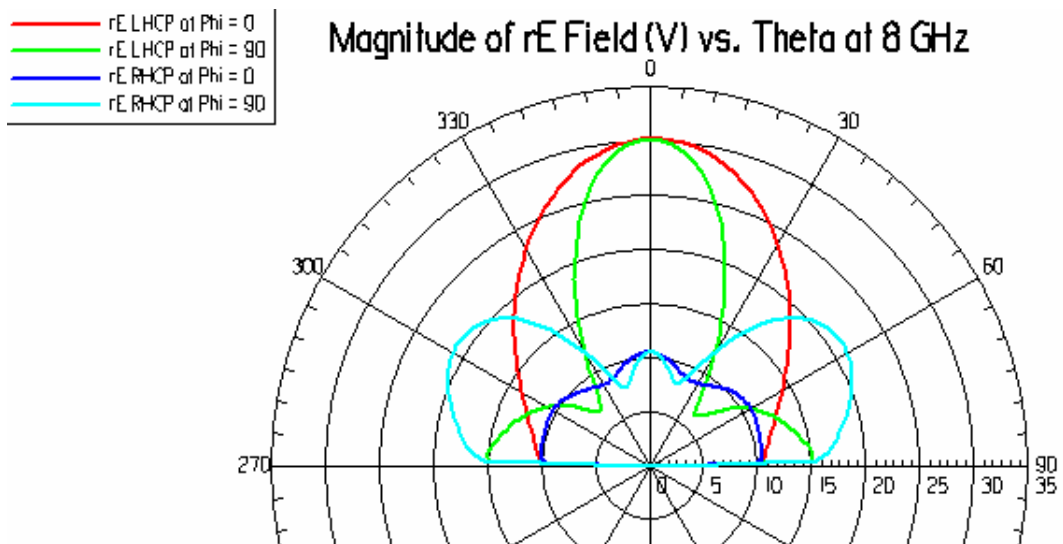

Figure 5–26 Far–field radiation pattern at 8 GHz
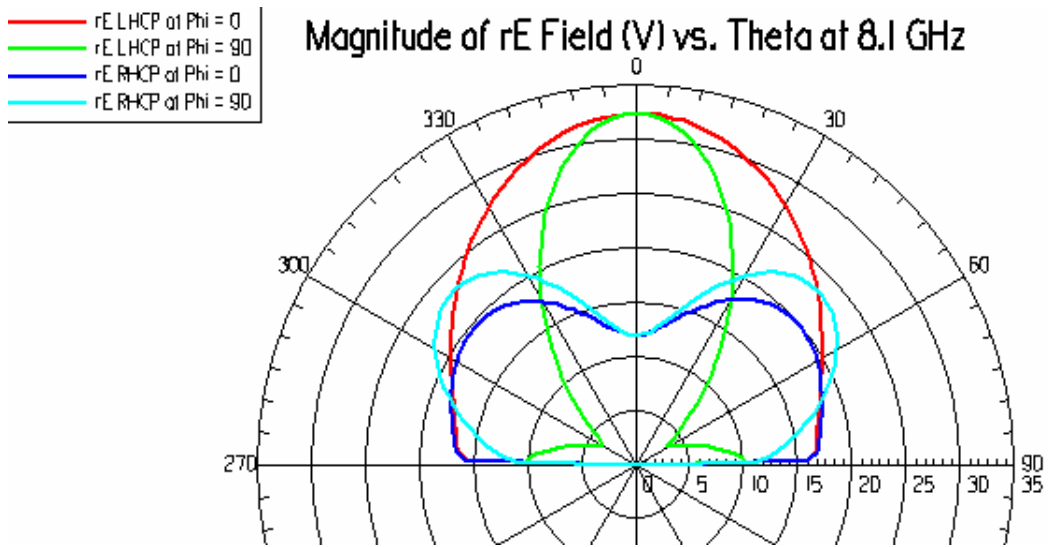
Figure 5–27 Far–field radiation pattern at 8.1 GHz
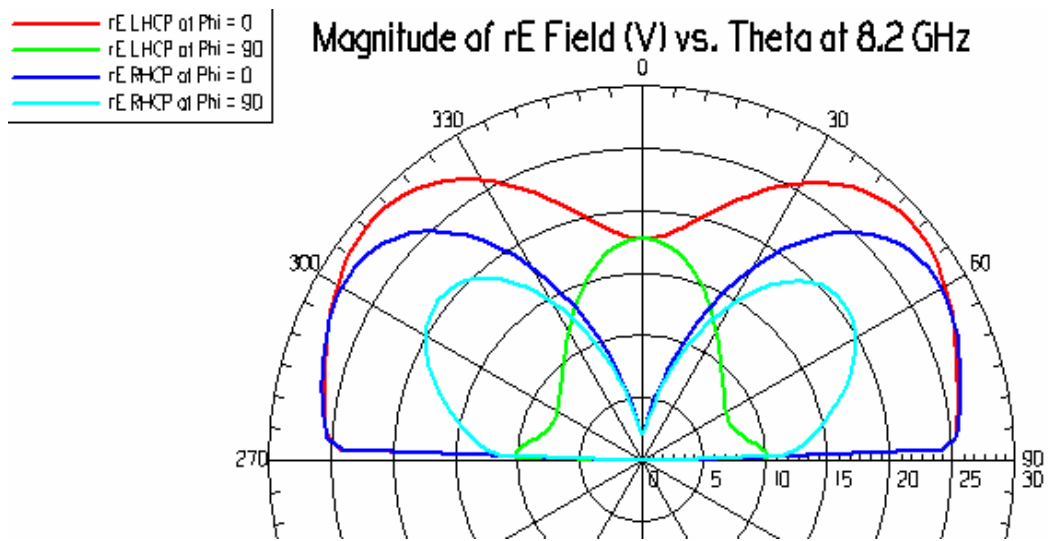
Figure 5–28 Far–field radiation pattern at 8.2 GHz

We get similar radiation patterns for one port feeding and two port feeding. The optimal operating frequency is seen from the scattering parameter graph as 8 GHz. At this frequency the efficiency was calculated as 98%. But the radiation pattern at this frequency is not the desired one. At 8.1 GHz. the radiation pattern is suitable for the desired LEO antenna specifications, however at this frequency the efficiency of the antenna decreases to 96% and also cross polarization is greater than normal polarization. The efficiency continues to decrease at 8.2 GHz., operating frequency of our antenna, to 82%, at that frequency the cross polarization is also greater than the normal polarization. These effects occur as a result of the merging of 8 ports to one single port.

In the previous examples the antenna substrate thickness was 0.127 mm. This is extremely thin substrate to fabricate without an error. By investigating laboratory equipment it has been decided to simulate the antenna with the RO4003 substrate material with an antenna layer thickness of 0.51 mm. Circular feed and annular feed sections use two different layers of the same substrate material, and thicknesses are 4 layers of 1.52 mm each. The relative permittivity of RO4003 is 3.38 and the tangential loss factor is 0.0027 (ε_r = 3.38 and a loss factor tanδ = 0.0027). Using these parameters, we simulated the antenna as correctly as possible before the fabrication. The substrate thicknesses adjusted so that the feeding lines can be produced practically.

To get ideal antenna pattern we again choose condition *c/b* = 2.5 and a RO4003 substrate material. For that *c/b* ratio, ξ_{12} = 2.2635. Substrate thickness is 0.51 mm. which is comparable to the wavelength at this operating frequency. This is a thickness that must be taken into account for fringing fields. For that condition we must find *a, b* and *c* values;

$$a = \frac{1.84118 \times 3 \times 10^8}{2\pi \times 8.2 \times 10^9 \sqrt{3.38}} m = 5.83 \text{ mm.}$$

$$b = \frac{2.2635 \times 3 \times 10^8}{2\pi \times 8.2 \times 10^9 \sqrt{3.38}} \, m. = 7.17 \text{ mm}.$$

c = 2.5 x 7.17 = 17.925 mm.

The above values are effective values, so exact physical values must be found using the formulas in [8],

$$a_e = a\left\{1 + \frac{2h}{\pi a \varepsilon_r}\left(\ln\frac{\pi a}{2h} + 1.7726\right)\right\}^{1/2}$$

$b_e = b - 3h/4$

$c_e = c + 3h/4$

Using these formulas, one calculates the physical dimensions as;

a = 5.61 mm.,

b = 7.55 mm.,

and *c* = 17.54 mm.

Using a similar methodology as in the previous case, the theoretical antenna dimensions are adjusted by using simulations. At the beginning, for the adjustment of the antenna dimensions, 8 different port feeding technique is used.

The circular section is fed with amplitude equal to 1, and annular section with amplitude equal to 0.2. The antenna, frequency response and the radiation pattern for 8, 8.1, 8.2 GHz are shown in Figs.5–29 through 5–32.
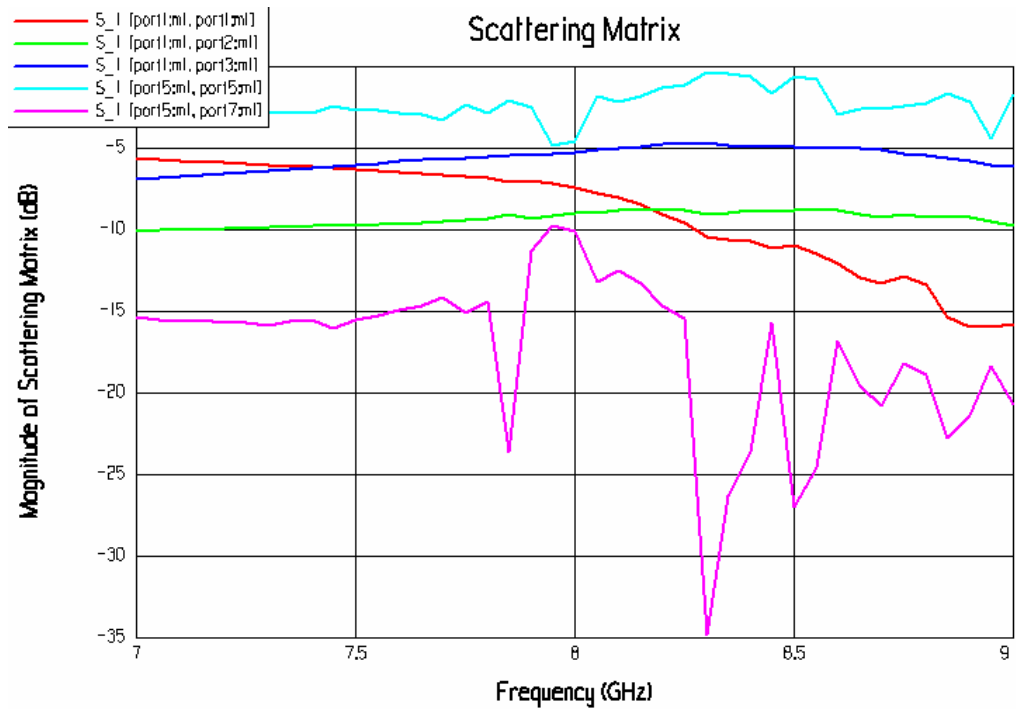
Figure 5–29 Scattering parameter graph of CDAR antenna (a=5,61 mm., b=7,55 mm. and 17,54 mm. ρ_{01}=3,5 mm., ρ_{02} =11 mm.)
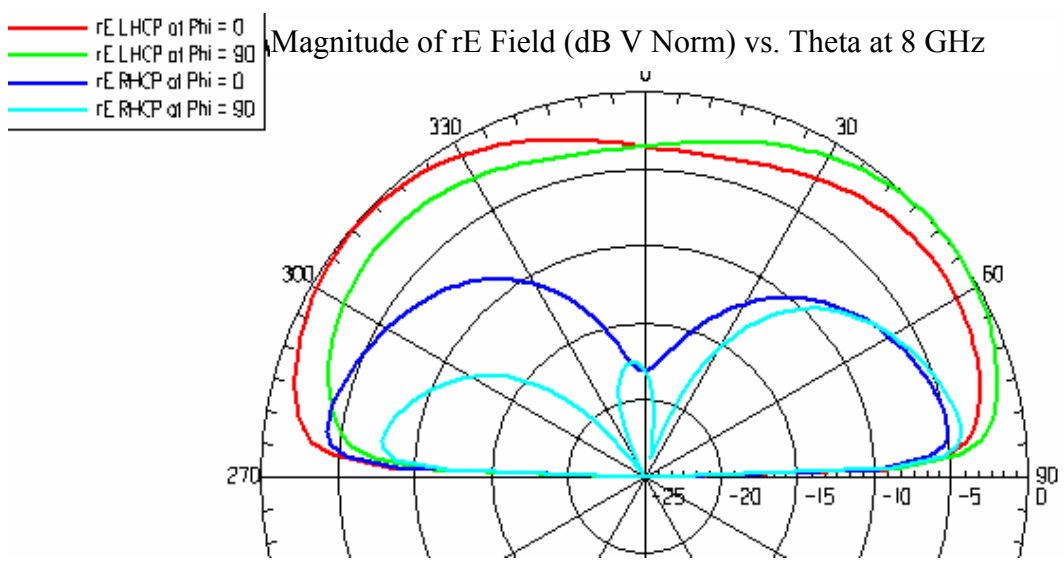

Figure 5–30 Far–field radiation pattern at 8 GHz.
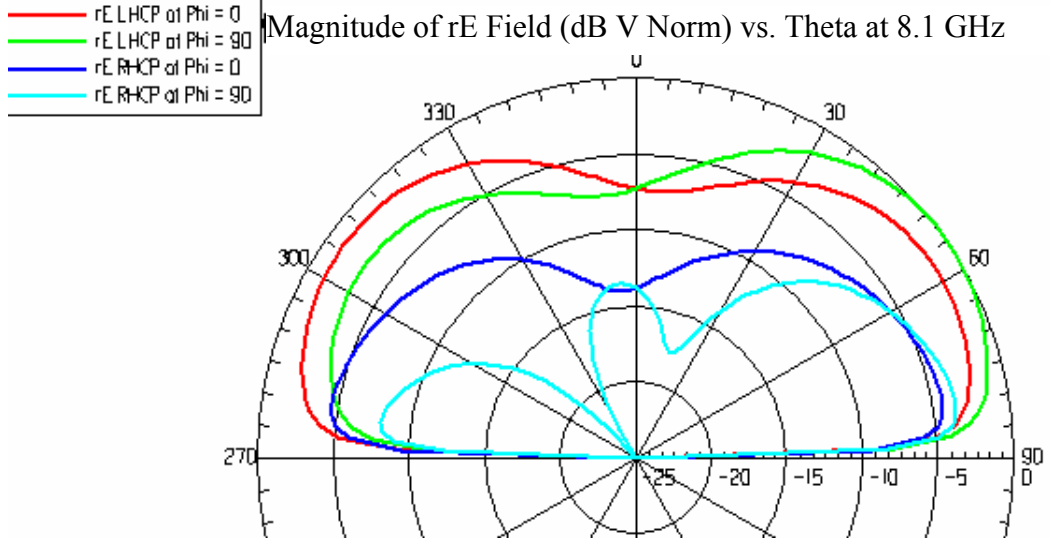
Figure 5–31 Far–field radiation pattern at 8.1 GHz.
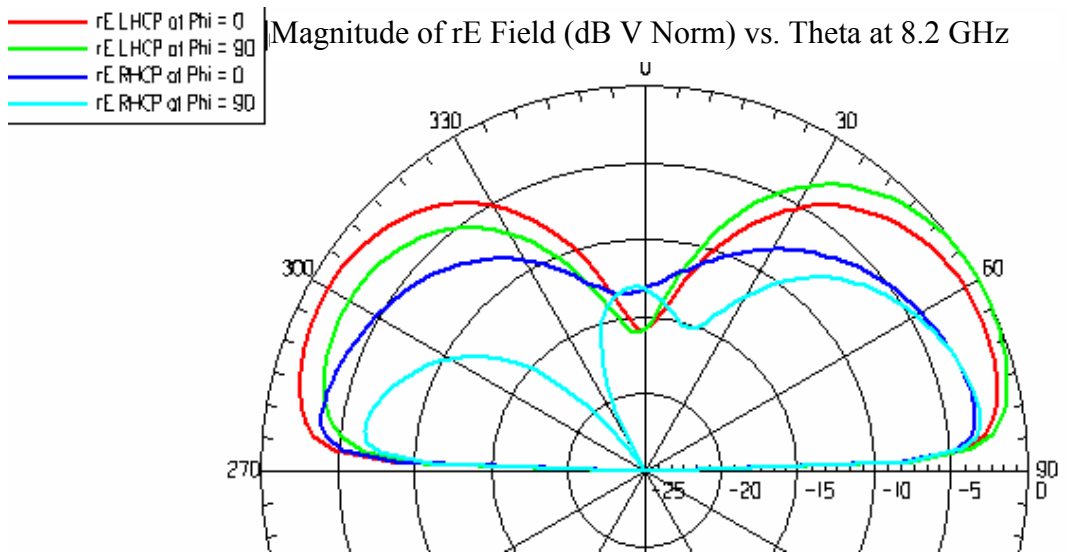
Figure 5–32 Far–field radiation pattern at 8.2 GHz.

Investigating the above graphs, we understand that the circular section and annular section resonance frequency is not 8.2 GHz., instead they have different frequencies, but the radiation pattern is similar to the desired pattern especially at 8.1 GHz. At that frequency the efficiency of the antenna is 84%. The radiation pattern decreases more at the top section of the antenna at 8.2 GHz with a greater efficiency of 86%. Similar is the pattern, however, the efficiency decreases to 82% at 8.0 GHz. At other frequencies radiation patterns differ largely from our desired pattern.

By making some adjustment we attempted to get a resonance frequency at 8.2 GHz. For a=6,1 mm, b=7,5 mm, c=17,4 mm, ρ_{01}=3,5 mm and ρ_{02} =11 mm, the scattering parameter and far field radiation patterns are shown in the Fig.5–33 and 5–34 respectively.
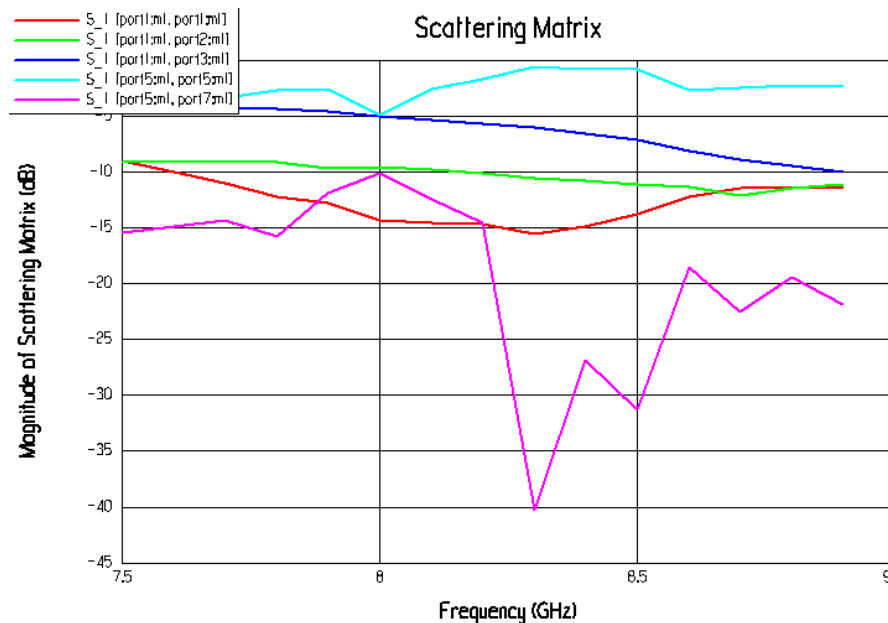
Figure 5–33 Scattering parameter graph
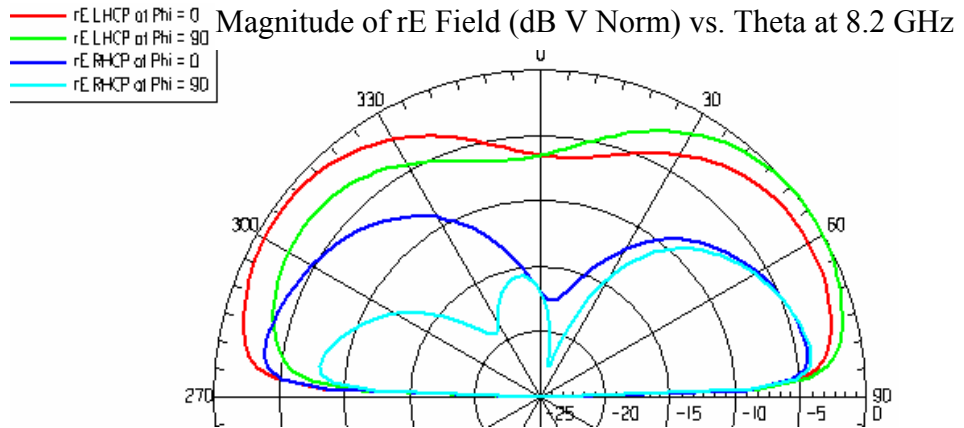
Figure 5–34 Far–field radiation pattern at 8.2 GHz.

According to the above simulation results we followed a similar methodology as in the previous case to feed the antenna from only one port. We get antenna shape, scattering parameter and far field radiation patterns at different frequencies as shown in Figs.5–35 through 5–40. At some frequencies the efficiency of the antenna is given in Table 5–1 below.

Table 5–1 The efficiency of the antenna at some frequencies

f (GHz)	P_{in} (W)	P_{out} (W)	e (Efficiency)
8.10	49.44	48.71	0.98
8.15	49.44	48.75	0.99
8.20	49.44	48.39	0.98
8.25	49.44	48.45	0.98
8.30	49.44	47.89	0.97
8.35	49.44	47.30	0.96
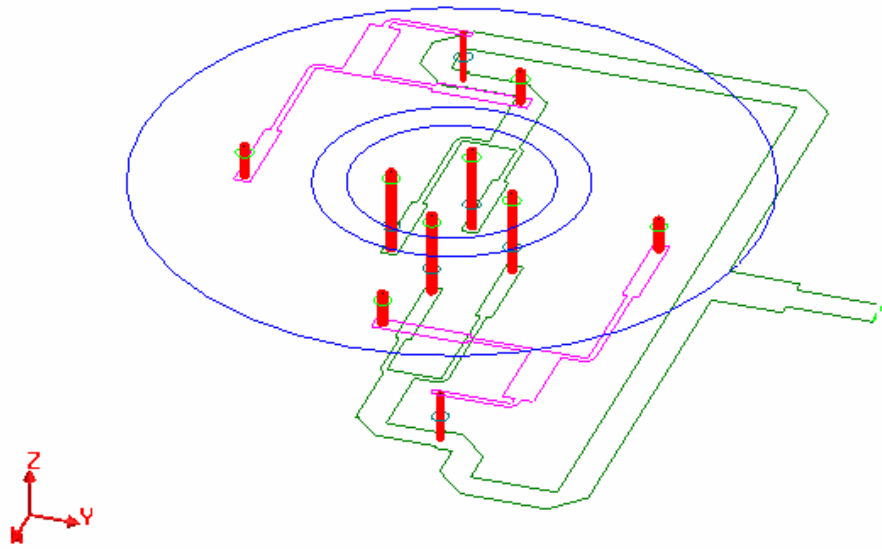
Figure 5–35 Antenna 3–dimensional view
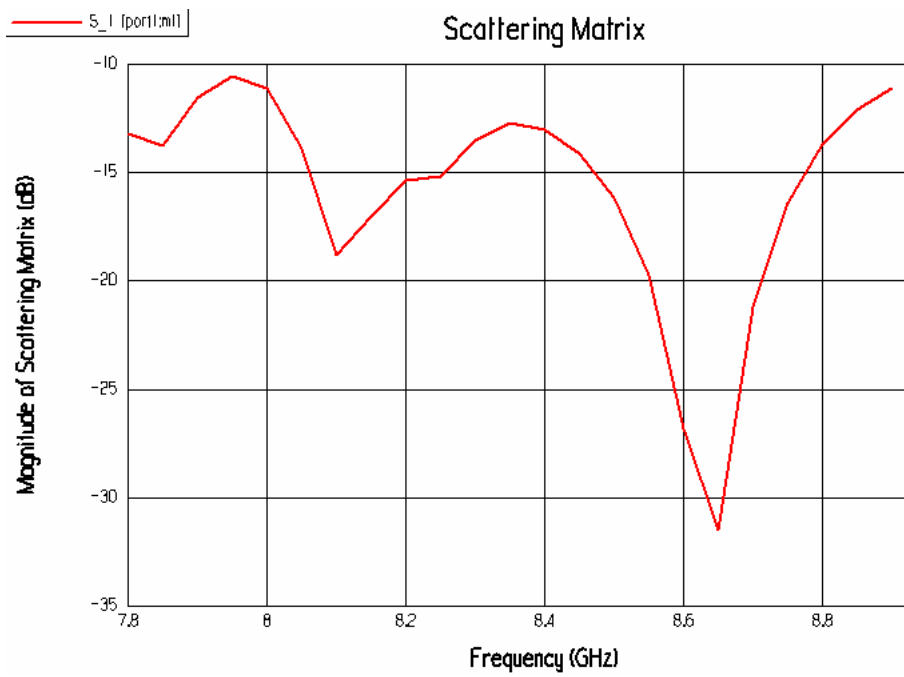
Figure 5–36 Scattering parameter versus frequency graph
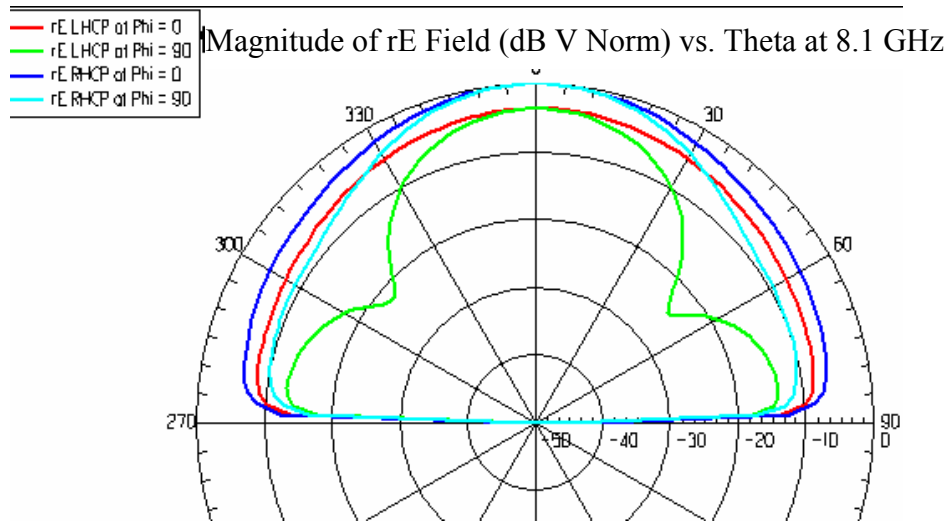
Figure 5–37 Far–field radiation pattern at 8.1 GHz
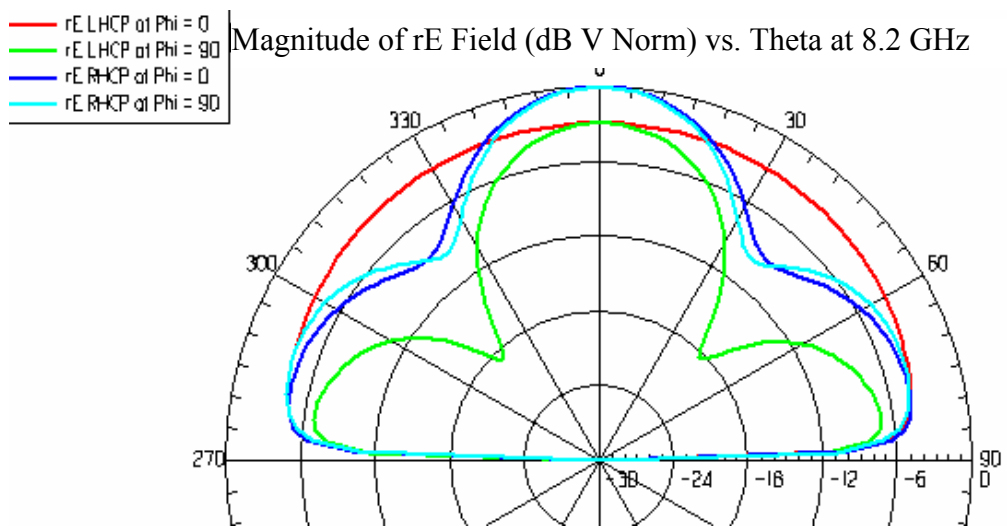
Figure 5–38 Far–field radiation pattern at 8.2 GHz

Contrary to the assumption that superposition principle is applicable, simulation program shows that there is a coupling between disk and annular section. This result can be seen in Figs.5–37 through 5–39.

57
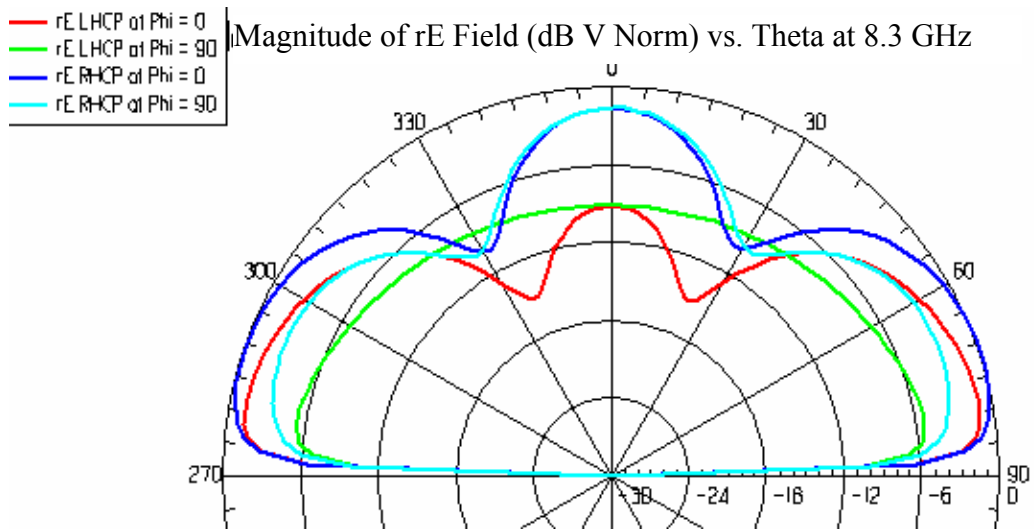
Figure 5–39 Far–field radiation pattern at 8.3 GHz
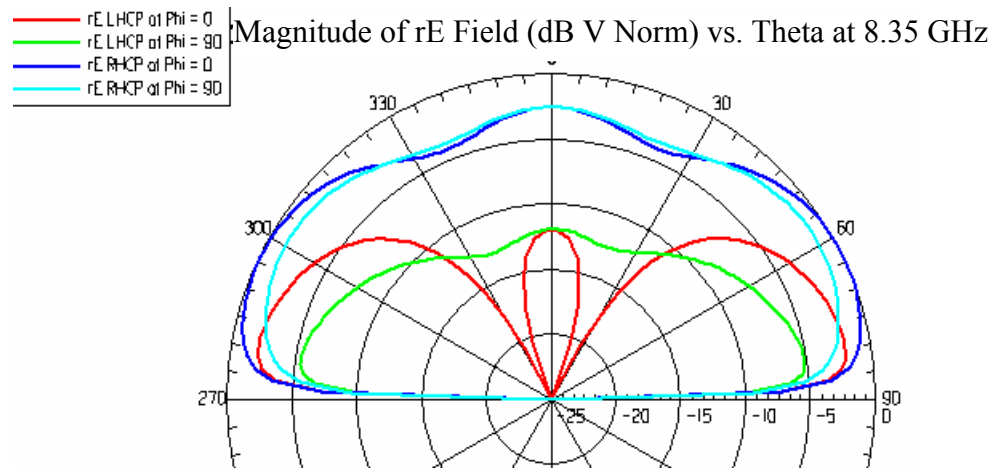
Figure 5–40 Far–field radiation pattern at 8.35 GHz.

The antenna pattern in Fig.5–40 can be considered as a sufficiently accurate approximation to the desired antenna pattern. (There is only a small discrepancy at the broadside direction). The cross polarization is about 10 dB below from the normal polarization at the region of interest. Dimensions for that antenna are

a=5.8 mm, b=7.7 mm, c=17.9 mm, ρ_{01}=*3.5 mm* and ρ_{02} =*12 mm*. The efficiency of the antenna at 8.35 GHz. is 96%, so it is an acceptable percentage.

The above values can be used to fabricate the antenna. The next section gives the experimental results.

5.2. Experimental Results:

We design the antenna as; *a=5.8 mm, b=7.7 mm, c=17.9 mm,* ρ_{01}=*3.5 mm* and ρ_{02} =*12 mm.* These are the same parameters as the last simulation results with Ansoft Ensemble 8.0 software. The designed antenna, feeding lines and ground planes are drawn by using AutoCAD drawing program, as shown in Fig.5–41.
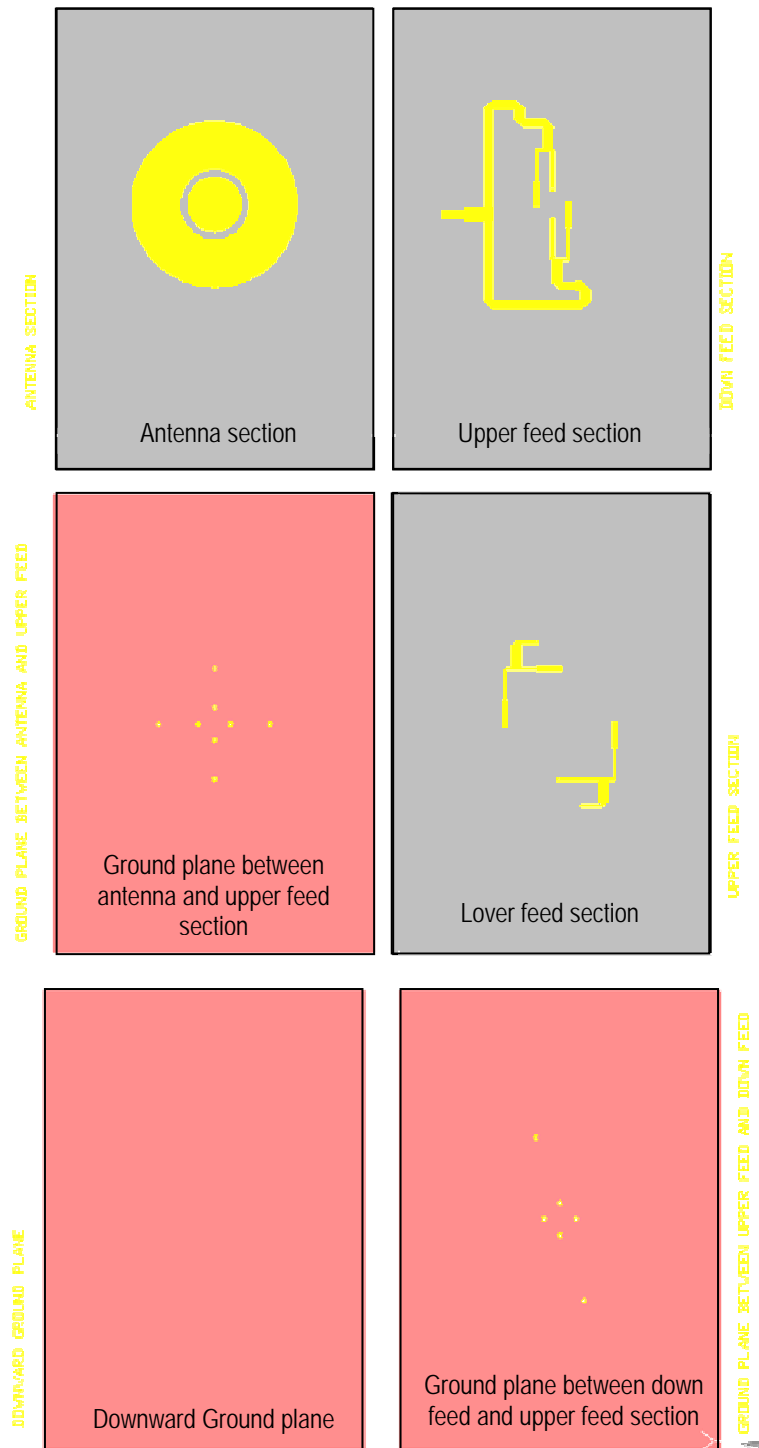
Figure 5–41 The Drawing of the antenna design used in the experimental analysis.

(All dimensions can be found in the diskette attached to this thesis.)
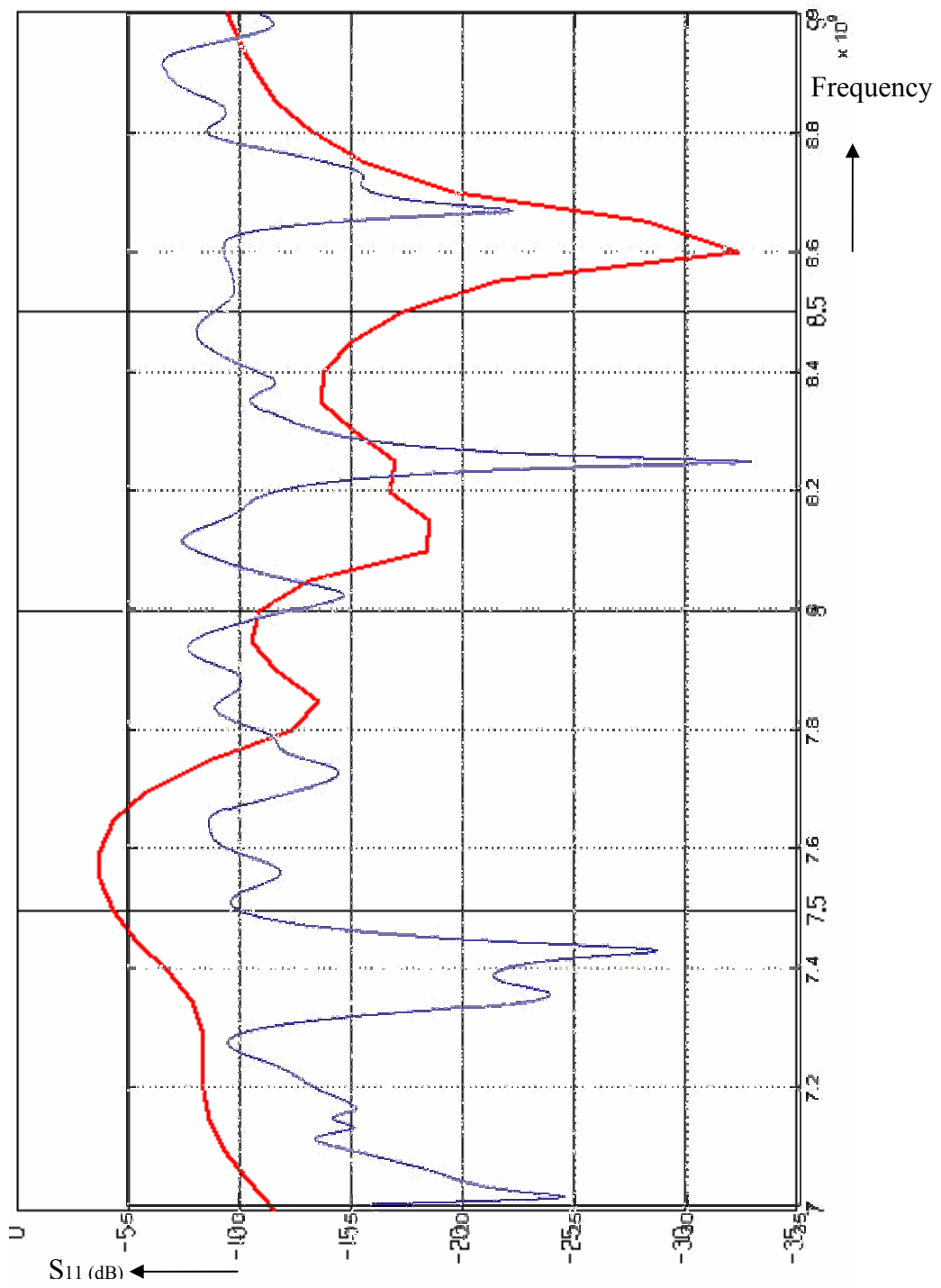
Figure 5–42 Comparison between experimental and simulation results (Scattering parameter,——— experimental, ——— simulation with Ansoft Ensemble 8.0)

Magnitude of rE Field (dB V Norm) vs. Theta at 8.35 GHz
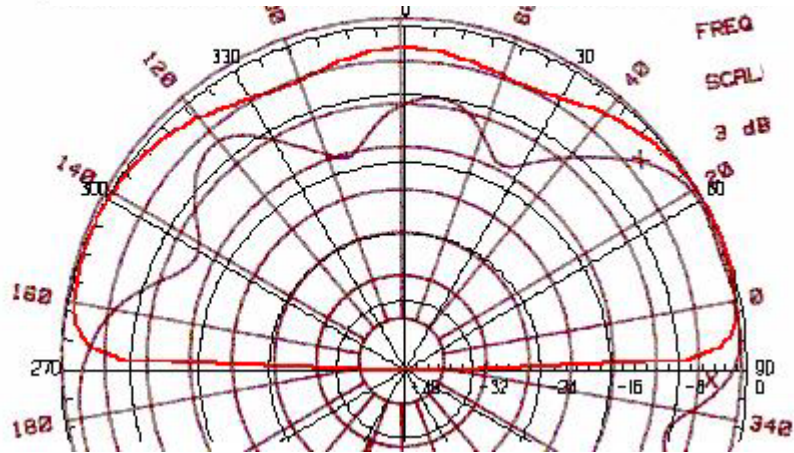
——————— Experimental result at 8.30 GHz. Vertical pattern

——————— Simulation results at 8.35 GHz

Figure 5–43 Far–field radiation pattern

Magnitude of rE Field (dB V Norm) vs. Theta at 8.35 GHz
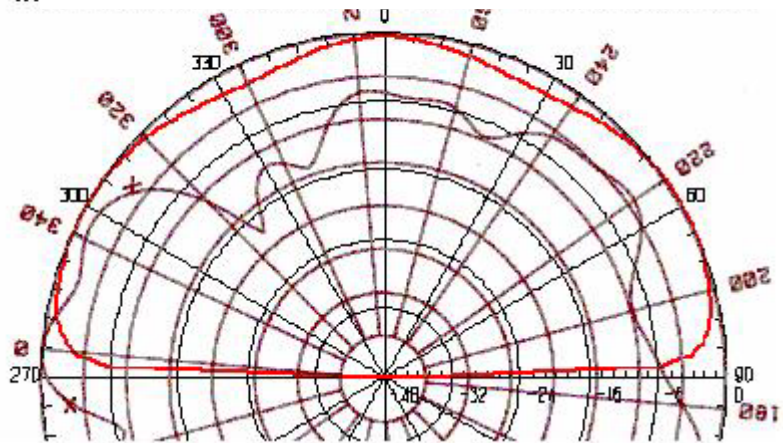
——————— Experimental result at 8.30 GHz. horizontal pattern

——————— Simulation results at 8.35 GHz

Figure 5–44 Far–field radiation pattern

Magnitude of rE Field (dB V Norm) vs. Theta at 7.4 GHz.
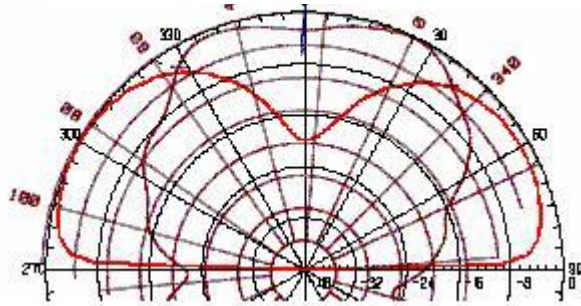
——————— Experimental result at 7.4 GHz. vertical pattern
————— Simulation results at 7.4 GHz

Figure 5–45 Far–field radiation pattern at 7.4 GHz.

Magnitude of rE Field (dB V Norm) vs. Theta at 7.4 GHz.
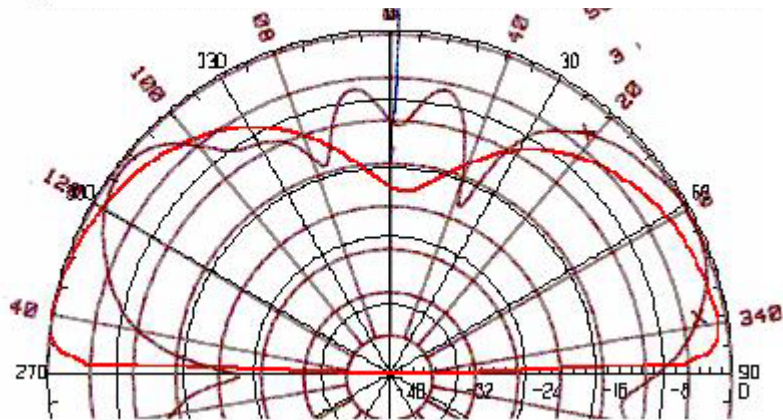
——————— Experimental result at 7.4 GHz. horizontal pattern
————— Simulation results at 7.4 GHz

Figure 5–46 Far–field radiation pattern at 7.4 GHz.

Magnitude of rE Field (dB V Norm) vs. Theta at 8.6 GHz.

—————— Experimental result at 8.6 GHz. vertical pattern
—————— Simulation results at 8.6 GHz
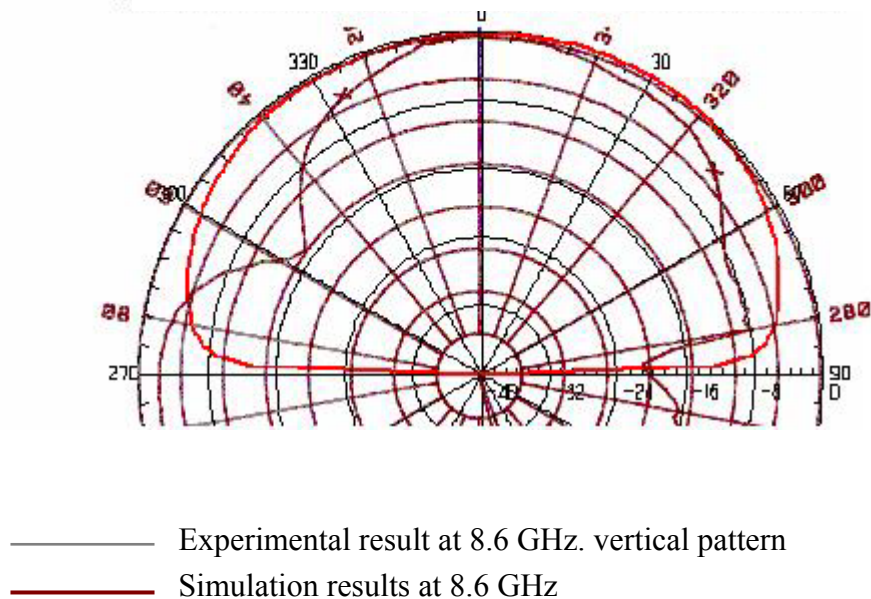
Figure 5–47 Far–field radiation pattern at 8.6 GHz.

5.3 Comparison and Discussions

Investigating the simulation and the experimental results; we see from the scattering parameter graph that these are roughly similar, but there are some discrepancies. Especially at 7.4 GHz the experimental antenna has a resonance, but that resonance can not be seen in the simulation. At 8.24 GHz. which is the best resonance of the overall antenna system, the experiment results show better matching conditions than that of the simulation. The best match between the simulation and experimental results occur at 8.6 GHz.

Investigating the far–field radiation graphs; the experimental results at 7.4 GHz vertical pattern is suitable for the LEO satellite antenna, but the horizontal pattern is not adequate. Simulation results at that frequency show that the amount of energy radiated in the broadside direction is much smaller. At 8.3 GHz. the far field radiation graphs show us little similarity between experimental and simulation results that is very close to the specified frequency of 8.2 GHz. At 8.6

64

GHz. best similarity at far field radiation graphs between experiment and simulation results is obtained.

The reason for the discrepancies between the experiment and simulation may possibly be due to the formulation characteristics of the simulation program. Another important factor may be the effect of the coupling between feeding probes in the finalized design. And the other factor may be the cause of implementation problems during fabrication period. It can be seen that the chosen parameters are not suitable for proper operation.

Feeding from one port, instead of feeding from eight different ports, may have caused this result. Studies have to continue in this matter.

The next section presents the conclusion of the thesis.

CHAPTER 6

CONCLUSION

The aim of this study is to design an antenna at 8.2 GHz for a LEO satellite. The desired antenna pattern is shown in Fig.1–1. We have chosen a microstrip structure for this design. The antenna is considered to compose of two main parts; a circular disk at the center and an annular ring at the outer section.

By means of a theoretical analysis, it has been concluded that the circular and annular disks must operate at TM_{11} and TM_{12} modes respectively.

In this study, an 8 port feeding structure is, first, simulated using Ansoft Ensemble 8.0 software program. In this structure, all ports are assumed to be fed separately and the desired antenna pattern is achieved by adjusting the magnitudes of inner and outer section feedings. By doing so, we could get different radiation patterns which are all suitable for the LEO satellite antenna.

But, 8 ports feeding is difficult to implement for users and requires that all probes have different phases and magnitudes. In order to simplify the feeding of the antenna, we tried to combine all 8 ports to a single feeding point. While combining the ports we adjusted their phases and magnitudes for the desired radiation condition by using microstrip line sections.

The combination of ports to a single feeding point, however, resulted in some problems: Although simulation results yielded appropriate (or at least acceptable) radiation shapes as long as LEO satellite antenna specifications are considered, experimental results failed. The deviation from the desired antenna pattern in experimental results can be related to following factors: In the simulation program, the ground plane is assumed to be infinite whereas it is finite in the experiments. In

addition, the thickness of the feeding probes is assumed to be zero in simulations; but, in reality, they have some thickness. If we make an assessment that a single probe yields a contribution of 5% deviation from the desired antenna pattern, the total deviation for an 8 port feeding structure would certainly be much higher.

A possible solution to the problem stated above would be the implementation of an electronic circuit at the bottom of the antenna section to feed the antenna emulations on 8 probe feeding. Another solution might be the use of a hybrid circuit. The investigation of these suggestions is left as future works.

REFERENCES

[1] H.Kawakami, G.Sato and R.Wakabayashi, *"Research on Circularly Polarized Conical Beam Antennas"*, IEEE Antennas and Propagation Magazine, Vol.39, No.3, pp.27-37, June 1997.

[2] J.Huang, *"Circularly Polarized Conical Pattern from Circular Microstrip Antennas"*, IEEE Transactions on Antennas and Propagation, Vol.AP-32, No.9, pp.991-994, September 1984.

[3] N.J.McEvan, R.A.Abd-Alhameed, E.M.Ibrahim, P.C.Excell and J.G.Gardiner, *"A New Design of Horizontally Polarized and Dual Polarized Unipolar Conical Beam Antennas for HIPERLAN"*, IEEE Transactions on Antennas and Propagation, Vol.51, No.2, pp.229-237, February 2003.

[4] R.Cahill, I.Cartmell, G.Van Dooren, K.Clibbon and C.Sillence, *"Performance of Shaped Beam Quadrifilar Antennas on the METOP Spacecraft"*, IEE Proc.-Microw. Antennas Propag., Vol.145, No.1, pp.19-24, February 1998.

[5] P. Bhartia, I. Bahl, R. Garg, A. Ittipiboon, *"Microstrip Antenna Design Handbook"*, Artech House Antennas and Propagation Library, pp.2-43, 2001.

[6] H.M.Chen and K.L.Wong, *"On the Circular Polarization Operation of Annular-ring Microstrip Antennas"*, IEEE Transactions on Antennas and Propagation, Vol.47, No.8, pp.1289-1292, August 1999.

[7]   A.K.Bhattacharyya and R.Grag, *"Input Impedance of Annular Ring Microstrip Antenna Using Circuit Theory Approach"*, IEEE Transactions on Antennas and Propagation, Vol.AP-33, No.4, pp.369-374, April 1985.

[8]   M.Tanaka and N.Takahashi, *"Suppressing Undesired Modes in a Higher Order Mode Microstrip Ring Patch Antenna"*, Electronics and Communications in Japan, Part 1, Vol.85, No.3, pp.9-18, 2002.

[9]   A.K.Bhattacharyya and L.Shafai, *"A Wider Band Microstrip Antenna for Circular Polarization"*, IEEE Transactions on Antennas and Propagation, Vol.36, No.2, pp.157-163, February 1988.

[10] K.Tamakuma and H.Iwasaki, *"A Small Size Circularly Polarized Annular Microstrip Antenna"*, IEEE 0-7803-7846-6/03/$17.00, pp.716-719, 2003.

[11] P. Bhartia, I. Bahl, R. Garg, A. Ittipiboon, *"Microstrip Antenna Design Handbook"*, Artech House Antennas and Propagation Library, pp.317-386, 2001.

APPENDIX –A

GENERAL DESCRIPTIONS OF MICROSTRIP ANTENNAS

Radiation from a rectangular patch can be explained with the fields that occur between the patch metallization and the ground plane. [5]
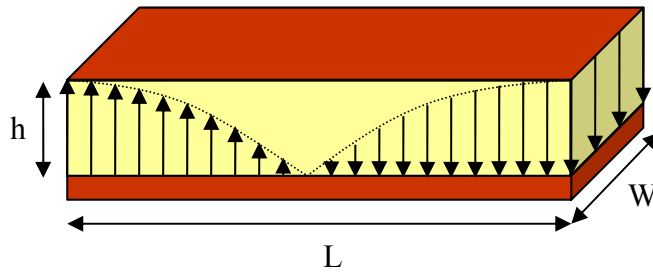
Figure A–1 Electric field distributions in the microstrip cavity

Practical microstrip antennas have small h/W ratio. To simply explain the field distribution, let's assume that no fields variation along h. (assume $h \ll \lambda$) As a result the patch can be modeled as a cavity. The electric field lines of TM_{100} modes are plotted in Fig.2–2. Equivalent currents are;

$$\vec{J}_s = \hat{n} \times \vec{H}_a \tag{A.1.a}$$

$$\vec{M}_s = -\hat{n} \times \vec{E}_a \tag{A.1.b}$$

Ground plane effect can be taken into account by image theory, this will double the magnetic current density in (2.1.b), while the image of the electric current density will be in opposite direction and cancel. Thus the current density will be;

$$\vec{M}_s = -2\hat{n} \times \vec{E}_a \tag{A.2}$$

The electric field for the dominant mode, as shown in Fig.2–2., is given by:

$$\vec{E}_a = \hat{z}E_o \tag{A.3}$$

for the slots of height h and length W. Similarly for the other slot the electric field can be written as;

$$\vec{E}_a = -\hat{z}E_0 \sin(\pi x / L) \tag{A.4}$$

From Fig.2–2; the radiation from slots that laid along $x-$ axis is almost zero, because the same amplitude but opposite currents. The only fields that radiate from the slots that laid along $y-$ axis.

Electric and magnetic fields at any point outside the microstrip antenna region can be written as:

$$\vec{E}^m(r) = -\frac{1}{\varepsilon} \nabla \times \vec{F} \tag{A.5}$$

$$\vec{H}^m(r) = \frac{1}{j\omega\mu\varepsilon} \nabla(\nabla \cdot \vec{F}) - j\omega\vec{F} \tag{A.6}$$

$$\vec{F} = \frac{\varepsilon}{4\pi} \iint_S \overline{M}(\bar{r}') \frac{e^{-jk_0|\bar{r}-\bar{r}'|}}{|\bar{r}-\bar{r}'|} dS' \tag{A.7}$$

71

where;

ε is the permittivity of the medium,

μ is the permeability of the medium,

k_0 is the free space wave number,

$\overline{M}(\overline{r}')$ is the surface magnetic current density at a point $\overline{r}'$ on the surface of the patch as shown in Fig.2–3 below.
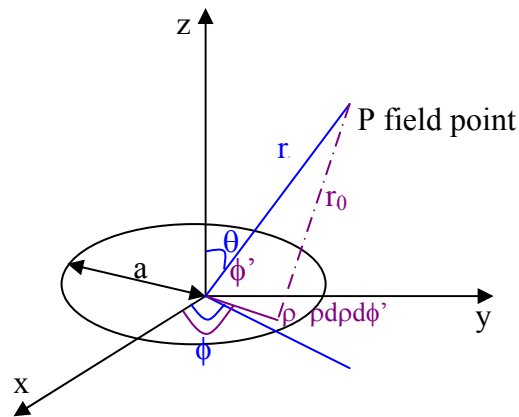
Figure A–2 Source of current sheet

Similar methods can be used to write the fields due to an electric current,

$$\overset{\rho}{E}^e(r) = \frac{1}{j\omega\mu\varepsilon}\nabla(\nabla \cdot \overset{\rho}{A}) - j\omega\overset{\rho}{A} \tag{A.8}$$

$$\overset{\rho}{H}^e(r) = \frac{1}{\mu}\nabla \times \overset{\rho}{A} \tag{A.9}$$

where;

$$\vec{A} = \frac{\mu}{4\pi} \iint_S \vec{J}(\vec{r}') \frac{e^{-jk_0|\vec{r}-\vec{r}'|}}{|\vec{r}-\vec{r}'|} dS' \tag{A.10}$$

Total fields can be written as;

$$\vec{E} = \vec{E}^e + \vec{E}^m = \frac{1}{j\omega\mu\varepsilon}\nabla(\nabla \cdot \vec{A}) - j\omega\vec{A} - \frac{1}{\varepsilon}\nabla \times \vec{F} \tag{A.10}$$

$$\vec{H} = \vec{H}^e + \vec{H}^m = \frac{1}{j\omega\mu\varepsilon}\nabla(\nabla \cdot \vec{F}) - j\omega\vec{F} + \frac{1}{\mu}\nabla \times \vec{A} \tag{A.11}$$

The important field components in the far field region are the θ and φ components, that are transverse to the direction of propagation.

For magnetic current alone;

$$H_\theta = -j\omega F_\theta \text{ and } H_\phi = -j\omega F_\phi,$$

in free space;

$$\vec{E} = -\eta_0 \hat{r} \times \vec{H} = -\eta_0(\hat{\phi}H_\theta - \hat{\theta}H_\phi) = j\omega\eta_0(\hat{\phi}F_\theta - \hat{\theta}F_\phi) \tag{A.12}$$

Where η_0 is the free space impedance = 120π,

For electric current alone;

$$E_\theta = -j\omega A_\theta, \ E_\phi = -j\omega A_\phi$$

73

$$\overset{\rho}{H} = \hat{r} \times \frac{\overset{\rho}{E}}{\eta_0}$$

In the far – field, the phase term is approximated by;

$$\left|\bar{r} - \bar{r}'\right| = r - r' \cos\phi \text{ in the numerator, while}$$

$$\left|\bar{r} - \bar{r}'\right| \approx r \text{ in the denominator, this gives us;}$$

$$\overset{\rho}{F} \cong \frac{\varepsilon}{4\pi} \frac{e^{-jk_0 r}}{r} \iint_S \overset{\rho}{M}(r') e^{jk_0 r' \cos\phi} ds' \tag{A.13}$$

$$\overset{\rho}{A} \cong \frac{\mu}{4\pi} \frac{e^{-jk_0 r}}{r} \iint_S \overset{\rho}{J}(r') e^{jk_0 r' \cos\phi} ds' \tag{A.14}$$

In our studies we make a circular and annular antenna, so let's formulate for a circular antenna that shown in the Fig.A–2. Far – field vector magnetic potential is [5];

$$\overset{\rho}{A} = \frac{\mu_0}{4\pi} \frac{e^{-jk_0 r}}{r} \int_0^{2\pi}\int_0^a J(\rho,\phi') \exp[jk_0\rho\sin\theta\cos(\phi'-\phi)]\rho d\rho d\phi' \tag{A.15}$$

Surface current density in polar coordinates is; $\overset{\nu}{J}(\rho,\phi') = J_\rho(\rho,\phi')\hat{\rho} + J_\phi(\rho,\phi')\hat{\phi}$

$$\overset{\rho}{A} = \frac{\mu_0}{4\pi} \frac{e^{-jk_0 r}}{r} \int_0^{2\pi}\int_0^a \left\{ J_\rho(\rho,\phi')\hat{\rho} + J_\phi(\rho,\phi')\hat{\phi} \right\} \exp[jk_0\rho\sin\theta\cos(\phi'-\phi)]\rho d\rho d\phi' \tag{A.16}$$

$$A_\theta = \frac{\mu_0}{4\pi} \frac{e^{-jk_0 r}}{r} \cos\theta \int_0^{2\pi}\int_0^a \left\{ J_\rho(\rho,\phi')\cos(\phi'-\phi) \right.$$

$$-J_\phi(\rho,\phi')\sin(\phi'-\phi)\Big\}\exp[jk_0\rho\sin\theta\cos(\phi'-\phi)]\rho d\rho d\phi' \quad \text{(A.17a)}$$

$$A_\phi = \frac{\mu_0}{4\pi}\frac{e^{-jk_0r}}{r}\int_0^{2\pi}\int_0^a \Big\{J_\rho(\rho,\phi')\sin(\phi'-\phi)$$

$$-J_\phi(\rho,\phi')\cos(\phi'-\phi)\Big\}\exp[jk_0\rho\sin\theta\cos(\phi'-\phi)]\rho d\rho d\phi' \quad \text{(A.17b)}$$

Similar expressions can be derived for the vector electric potential F_θ and F_ϕ

$$F_\theta = \frac{-\epsilon_0}{4\pi}\frac{e^{-jk_0r}}{r}\cos\theta\int_0^{2\pi}\int_\rho M_\phi(\rho,\phi')\sin(\phi'-\phi)\exp[jk_0\rho\sin\theta\cos(\phi'-\phi)]\rho d\rho d\phi'$$

$$\text{(A.18a)}$$

$$F_\phi = \frac{\epsilon_0}{4\pi}\frac{e^{-jk_0r}}{r}\int_0^{2\pi}\int_\rho M_\phi(\rho,\phi')\cos(\phi'-\phi)\exp[jk_0\rho\sin\theta\cos(\phi'-\phi)]\rho d\rho d\phi' \quad \text{(A.18b)}$$

$$E_\theta = -j\omega\eta_0 F_\phi$$

$E_\phi = -j\omega\eta_0 F_\theta$ Using (A.18a) and (A.18b), we can write,

$$E_\theta = \frac{-jk_0}{4\pi}\frac{e^{-jk_0r}}{r}\int_0^{2\pi}\int_\rho (M_\phi(\rho,\phi')\cos(\phi'-\phi)\exp[jk_0\rho\sin\theta\cos(\phi'-\phi)]\rho d\rho d\phi'$$

$$\text{(A.19a)}$$

$$E_\phi = \frac{-jk_0}{4\pi}\frac{e^{-jk_0r}}{r}\cos\theta\int_0^{2\pi}\int_\rho (M_\phi(\rho,\phi')\sin(\phi'-\phi)\exp[jk_0\rho\sin\theta\cos(\phi'-\phi)]\rho d\rho d\phi'$$

$$\text{(A.19b)}$$

Radiated power from a microstrip antenna can be calculated by integrating the Poynting vector over a closed surface as;

$$P_r = \frac{1}{2\eta_0} \text{Re} \iint\limits_{aperture} (\vec{E} \times \vec{H}^*) \cdot d\overline{S}$$ and in the microstrip antenna region electric field

is normal to the patch and ground plane, magnetic field is parallel to strip so above formula can be written as;

$$P_r = \frac{1}{2\eta_0} \iint (|E_\theta|^2 + |E_\phi|^2) r^2 \sin\theta d\theta d\phi \tag{A.20}$$

Dissipated power in a microstrip antenna can be calculated by the sum of conductor loss and the dielectric loss.

Conductor loss is

$$P_c = R_s \iint\limits_S (\overline{J} \cdot \overline{J}^*) dS$$

R_s is the real part of the surface resistance of the patch the other comes from the ground plane total can be calculated from the above formula.

The dielectric loss can be calculated using the formula below;

$$P_d = \frac{\omega \varepsilon''}{2} \iiint\limits_V |E|^2 dV = \frac{\omega \varepsilon''}{2} h \iint\limits_S |E|^2 dS$$ for thin substrate.

Where ω is the radian frequency, h is the substrate thickness and ε'' is the imaginary part of the complex permittivity of the substrate.

APPENDIX –B

CIRCULAR DISK MICROSTRIP ANTENNAS

Circular microstrip antennas can be analyzed using cavity model. [11]

The wave equation for the electric fields can be written as;

$$(\nabla^2 + k^2)\vec{E} = 0 \qquad k = 2\pi\sqrt{\varepsilon_r} / \lambda_0 \qquad (B.1)$$

In side the cylindrical coordinate system, the wave equation,

$$E_z = E_0 J_n(k\rho)\cos n\phi \qquad (B.2)$$

$J_n(k\rho)$ are the Bessel functions of order n.

Because the electric field component has only a z – component and $\partial / \partial z = 0$, the magnetic field components becomes;

$$H_\rho = \frac{j}{\omega\mu\rho}\frac{\partial E_z}{\partial \phi} = -\frac{jn}{\omega\mu\rho}E_0 J_n(k\rho)\sin n\phi \qquad (B.3)$$

$$H_\phi = \frac{j}{\omega\mu}\frac{\partial E_z}{\partial \rho} = -\frac{jn}{\omega\mu}E_0 J_n'(k\rho)\cos n\phi \qquad (B.4)$$

$$E_\phi = \frac{-jk_0}{4\pi}\frac{e^{-jk_0 r}}{r}\cos\theta\int_0^{2\pi}\int_\rho (M_\phi(\rho,\phi')\sin(\phi'-\phi)\exp[jk_0\rho\sin\theta\cos(\phi'-\phi)])\rho d\rho d\phi'$$

$$(B.5)$$

We can use resonance approximation that only one mode contributes at a given frequency. To get an expression for the radiation fields we obtain the following;

$$E_\theta = \frac{-jk_0}{4\pi} \frac{e^{-jk_0r}}{r} E_n \int_0^{2\pi}\int_a^{a+h} J_n(\chi_{nm}\rho/a)\cos n\phi' \cos(\phi'-\phi)\exp[jk_0\rho\sin\theta\cos(\phi'-\phi)]\rho d\rho d\phi'$$

(B.6)

Using the approximate integration according to ρ, we get the following expression;

$$E_\theta = \frac{-jk_0}{4\pi} \frac{e^{-jk_0r}}{r} ahE_nJ_n(\chi_{nm})\int_0^{2\pi}\cos n\phi' \cos(\phi'-\phi)\exp[jk_0a\sin\theta\cos(\phi'-\phi)]d\phi'$$

(B.7)

$$\int_0^{2\pi}\cos n\phi' \cos(\phi'-\phi)\exp[jk_0a\sin\theta\cos(\phi'-\phi)]d\phi' = -2\pi(j)^{n+1}\cos n\phi J_n'(k_0a\sin\theta)$$

(B.8)

By using this expression we get;

$$E_\theta = \frac{-j^n k_0}{2}\frac{e^{-jk_0r}}{r} ahE_nJ_n(\chi_{nm})\cos n\phi J_n'(k_0a\sin\theta)$$ (B.9)

$$E_\theta = \frac{-j^n Vak_0}{2}\frac{e^{-jk_0r}}{r}\cos n\phi J_n'(k_0a\sin\theta)$$

$V = hE_nJ_n(\chi_{nm})$ is known as the edge voltage at $\phi=0$

To compute E_ϕ, the following useful integration can be used similarly;

$$\int_0^{2\pi} \cos n\phi' \sin(\phi' - \phi) \exp[jk_0 a \sin\theta \cos(\phi' - \phi)] d\phi' = 2\pi n(j)^{n+1} \sin n\phi \frac{J_n(k_0 a \sin\theta)}{k_0 a \sin\theta} \cos\theta$$

(B.10)

and we get;

$$E_\phi = nj^n \frac{Vak_0}{2} \frac{e^{-jk_0 r}}{r} \sin n\phi \frac{J_n(k_0 a \sin\theta)}{k_0 a \sin\theta} \cos\theta \qquad \text{(B.11)}$$

The effect of substrate material and the ground plane are not included in the above formulas. Some suitable correction factors must be taken into account for these effects. Following expressions are obtained;

$$E_\theta = \frac{-j^n Vak_0}{2} \frac{e^{-jk_0 r}}{r} \cos n\phi J_n{}'(k_0 a \sin\theta) F_1(\theta) \qquad \text{(B.12a)}$$

$$E_\phi = nj^n \frac{Vak_0}{2} \frac{e^{-jk_0 r}}{r} \sin n\phi \frac{J_n(k_0 a \sin\theta)}{k_0 a \sin\theta} \cos\theta \cdot F_2(\theta) \qquad \text{(B.12b)}$$

Where $F_1(\theta)$ and $F_2(\theta)$ are given below;

$$F_1(\theta) = \frac{2\cos\theta \sqrt{\varepsilon_r - \sin^2\theta}}{\sqrt{\varepsilon_r - \sin^2\theta} - j\varepsilon_r \cos\theta \cot(k_0 h \sqrt{\varepsilon_r - \sin^2\theta})} \qquad \text{(B.13a)}$$

$$F_2(\theta) = \frac{2\cos\theta}{\cos\theta - j\sqrt{\varepsilon_r - \sin^2\theta} \cot(k_0 h \sqrt{\varepsilon_r - \sin^2\theta})} \qquad \text{(B.13b)}$$

Field Excited by the Feed Source:

The feeding technique of a microstrip antenna by a coaxial feed is shown in Fig.B–1 below,

$$\overset{\rho}{J} = \hat{z} J_z(\phi_0) \frac{\partial(\rho - \rho_0)}{\rho_0}$$

$$J_z(\phi_0) = \begin{cases} I, & \pi - \Delta \langle \phi_0 \langle \pi + \Delta \\ 0, & \textit{elsewhere} \end{cases}$$
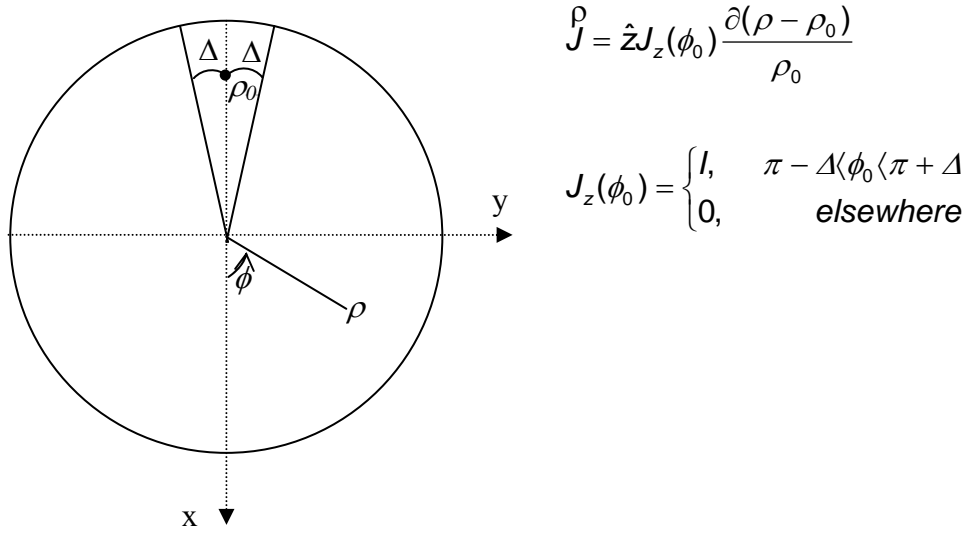
Figure B–1 Coaxial feed of a microstrip antenna

If there is a current source $\overline{J}$, The wave equation will be given by the following formulation;

$$\nabla^2 \overset{\rho}{E} + k^2 \overset{\rho}{E} = jw\mu \overset{\rho}{J} - \frac{\nabla(\nabla \cdot \overset{\rho}{J})}{jw\varepsilon}, \text{ where } \varepsilon = \varepsilon_0 \varepsilon_r \qquad \text{(B.14)}$$

Let's assume $\overline{J}$ and $\overline{E}$ has only z – component and no z – variation. According to that assumption;

$$\nabla \cdot \overset{\rho}{J} = \frac{\partial J_z}{\partial z} = 0$$

Using this assumption we get;

$$\nabla^2 E_z + k^2 E_z = jw\mu_0 \overset{\rho}{J}\hat{z} = jw\mu_0 J_z \qquad \text{(B.15)}$$

The solution of this equation in a circular circumstance;

$$E_z = \sum_n \sum_m A_{nm} \psi_{nm}(\rho, \phi) \qquad \text{(B.16a)}$$

$$(\nabla^2 + k_{nm}^2)\psi_{nm} = 0 \qquad \text{(B.16b)}$$

$$\frac{\partial \psi_{nm}}{\partial \rho}\Big|_{\rho=a} = 0 \qquad \text{(B.16c)}$$

Solutions of the above equations are;

$$\psi_{nm} = J_n(k_{nm}\rho)\cos n\phi \qquad \text{n=0, 1, 2, …,} \qquad \text{m=1, 2, 3, ….} \qquad \text{(B.17)}$$

$$A_{nm} = \frac{\iint \psi_{nm}^*(jw\mu_0 J_z)dS}{(k^2 - k_{nm}^2)\iint \psi_{nm}^*\psi_{nm}dS} \qquad \text{(B.18)}$$

$$A_{01} = jw\mu_0 I \frac{2\Delta}{\pi a^2 k^2} \qquad \text{n=0, m=1,} \qquad \text{(B.19a)}$$

$$A_{0m} = jw\mu_0 I \frac{2\Delta J_0(k_{0m}\rho_0)}{\pi a^2 J_0^2(k_{0m}a)(k^2 - k_{0m}^2)} \qquad \text{m}\geq 2, \text{ n=0,} \qquad \text{(B.19b)}$$

$$A_{nm} = jw\mu_0 I \frac{(-1)^n 4 \cdot \sin(n\Delta)J_n(k_{nm}\rho_0)k_{nm}^2}{n\pi(k^2 - k_{nm}^2)(k_{nm}^2 a^2 - n^2)J_n^2(k_{nm}a)} \qquad \text{n}\geq 1 \qquad \text{(B.19c)}$$

$$E_z = jw\mu_0 I \Bigg\{ \frac{2\Delta}{\pi a^2 k^2} + \sum_{m=2}^{\infty} \frac{2\Delta J_0(k_{0m}\rho_0)J_0(k_{0m}\rho)}{\pi a^2 J_0^2(k_{0m}a)(k^2 - k_{0m}^2)}$$

$$+ \sum_{n=1}^{\infty}\sum_{m=1}^{\infty} \frac{(-1)^n 4 \sin(n\Delta)J_n(k_{nm}\rho_0)J_n(k_{nm}\rho)k_{nm}^2 \cos n\phi}{n\pi(k^2 - k_{nm}^2)(k_{nm}^2 a^2 - n^2)J_n^2(k_{nm}a)} \Bigg\} \qquad \text{(B.20)}$$

81

The input impedance can be calculated as

$$Z_{in} = V_{in} / I_0$$

$$V_{in} = -E_{av}h,$$

$$E_{av} = \frac{1}{2\Delta} \int_{\pi-\Delta}^{\pi+\Delta} E_z(\rho_0, \phi) d\phi, \tag{B.21}$$

$$E_{av} = \frac{1}{2\Delta} \sum_n \sum_m A_{nm} J_{nm}(k_{nm}\rho_0) \int_{\pi-\phi}^{\pi+\phi} \cos n\phi d\phi$$

Z_{in} is calculated as the following expression in [11]

$$Z_{in} = -jw\mu_0 h \left\{ \frac{1}{\pi a^2 k^2(1-j\delta)} + \sum_{m=2}^{\infty} \frac{J_0^2(k_{0m}\rho_0)}{\pi a^2 J_0^2(k_{0m}a)[k^2(1-j\delta) - k_{0m}^2]} \right.$$

$$\left. + \frac{2}{\pi} \sum_{n=1}^{\infty} \sum_{m=1}^{\infty} (\frac{\sin n\Delta}{n\Delta})^2 \frac{J_n^2(k_{nm}\rho_0)}{J_n^2(k_{nm}a)} \frac{k_{nm}^2 \cos^2 n\phi_0}{[k^2(1-j\delta_{eff}) - k_{nm}^2](k_{nm}^2 a^2 - n^2)} \right\} \tag{B.22}$$

Input Impedance;

The input impedance is calculated from the formula;

$$Z_{in} = \frac{\frac{1}{2} V \cdot V^*}{P_T + 2jw(W_e - W_m)} \tag{B.23}$$

Where;

$$V = -\int_0^h E_z dz$$

82

$P_T=P_r+P_c+P_d$

If we assume n=1 mode is the dominant mode the voltage can be obtained as;

$$V = -A_1 h J_1(k\rho_0) \qquad (B.24)$$

$$P_r = \frac{1}{2}\pi a h |B_1 J_1(ka) + C_1 Y_1(ka)|^2 g_{s1} \qquad (B.25)$$

where;

$$g_{s1} = \frac{1}{k_0^2 a h \eta_0} \int_0^{\pi/2} (I_1^2 + I_2^2)\sin\theta d\theta \qquad (B.26)$$

$$I_1 = \frac{k_0 a \sin(k_0 h \cos\theta)}{\cos\phi} J_1'(k_0 a \sin\theta) \qquad (B.27a)$$

$$I_2 = \frac{\sin(k_0 h \cos\theta)}{\sin\theta} J_1(k_0 a \sin\theta) \qquad (B.27b)$$

$$P_c = \frac{2wW_m}{h\sqrt{\pi f \mu_0 \sigma}} \qquad (B.28)$$

$$P_d = 2wW_e \tan\delta \qquad (B.29)$$

$$W_e = \frac{\pi\varepsilon_0\varepsilon_r h}{8k^2}\{|A_1|^2 [x^2(J_1^2 - J_0 J_2)]_0^k \rho_0 + |B_1|^2 [x^2(J_1^2 - J_0 J_2)]_k^{ka} \rho_0 \qquad (B.30a)$$

$$+|C_1|^2 [x^2(Y_1^2 - Y_0 Y_2)]_k^{ka} \rho_0 + \frac{1}{2}(B_1 C_1^* + B_1^* C_1)[x^2(2Y_1 J_1 - J_0 Y_2 - J_2 Y_0)]_k^{ka} \rho_0\}$$

83

$$W_m = \frac{\pi\varepsilon_0\varepsilon_r h}{8k^2}\{|A_1|^2[x^2(J_0^2+J_1^2) - 2J_1^2]_0^k\rho_0 + |B_1|^2[x^2(J_0^2+J_1^2) - 2J_1^2]_k^{ka}\rho_0 \quad (B.30b)$$

$$+ |C_1|^2[x^2(Y_0^2+Y_1^2) - 2Y_1^2]_k^{ka}\rho_0$$

$$+ \frac{1}{2}(B_1C_1^* + B_1^*C_1)[x^2(2Y_0J_0 + J_1Y_1 + J_2Y_2 - \frac{1}{2}J_1Y_3 - -\frac{1}{2}J_3Y_1)]_k^{ka}\rho_0\}$$

Radiation Resistance

First of all we must calculate the radiated power, dielectric loss and copper loss, then we can calculate the radiation resistance for resonance condition.

$$P_d = \frac{w\varepsilon\tan\delta}{2}\iiint_v \vec{E}\cdot\vec{E}dv \qquad (B.31)$$

$$P_d = \frac{w\varepsilon\tan\delta E_0^2\pi h}{2}\int_{a_e}^{b_e}[J_n(k_{nm}\rho)Y_n'(k_{nm}a_e) - J_n'(k_{nm}a_e)Y_n(k_{nm}\rho)]^2\rho d\rho$$

$$P_d = \frac{w\varepsilon\tan\delta}{\pi}\left(\frac{E_0}{k_{nm}}\right)^2\left[\left(\frac{J_n'(k_{nm}a_e)}{J_n'(k_{nm}b_e)}\right)^2\left(1 - \frac{n^2}{k_{nm}^2 b_e^2}\right) - \left(1 - \frac{n^2}{k_{nm}^2 a_e^2}\right)\right]$$

Similarly for copper loss calculation;

$$P_c = 2\frac{R_s}{2}\int_a^b\int_0^{2\pi}\left(|J_\phi|^2 + |J_\rho|^2\right)\rho d\rho d\phi \qquad (B.32)$$

$$P_c = 2\frac{R_s}{\pi}\left(\frac{E_0}{w\mu_0}\right)^2\left[\left(\frac{J_n'(k_{nm}a)}{J_n'(k_{nm}b)}\right)^2\left(1 - \frac{n^2}{k_{nm}^2 b^2}\right) - \left(1 - \frac{n^2}{k_{nm}^2 a^2}\right)\right]$$

$$P_r = \frac{2wh}{\eta_0}\left(\frac{E_0 k_0}{k_{nm}}\right)^2 I_1 \tag{B.33}$$

Where I_1 is;

$$I_1 = \int_0^{\pi/2}\left[\frac{n^2\cos^2\theta}{k_0^2\sin\theta}\left(\frac{J_n(k_0 a\sin\theta)}{a} - \frac{J_n'(k_{nm}a)}{J_n'(k_{nm}b)}\frac{J_n(k_0 b\sin\theta)}{b}\right)^2\right. \tag{B.34}$$

$$\left. + \sin\theta\left(J_n'(k_0 a\sin\theta) - \frac{J_n'(k_{nm}a)}{J_n'(k_{nm}b)}J_n'(k_0 b\sin\theta)\right)^2\right]d\theta$$

We can use the above formulas to calculate the radiation resistance at resonance frequency as;

$$R_r = \frac{V_0^2}{2P_T}, \tag{B.35}$$

$P_T = P_r + P_c + P_d$, V_0 is the voltage at $\rho = b$ and $\phi = 0$.

Using the formulas one can derive the radiation resistance.

Directivity and Gain of a Circular Microstrip Disk Antenna;

Directivity D is calculated;

$$D = \frac{\frac{1}{2}\mathrm{Re}(E_\theta H_\phi^* - E_\phi H_\theta^*)\big|_{\theta=0}}{P_r\big/4\pi r^2} = \frac{\frac{r}{2\eta_0}(|E_\theta|^2 + |E_\phi|^2)\big|_{\theta=0}}{P_r\big/4\pi} \tag{B.36}$$

The gain of an antenna is calculated as; $G = e_r \cdot D$

Where e_r is the radiation efficiency of the antenna which is $0 < e_r < 1$ and calculated by the formula;

$$e_r = \frac{P_r}{P_i} = \frac{P_r}{P_r + P_c + P_d + P_{sur.}} \qquad (B.37)$$